Photocatalytic Degradation of Water Pollutants Using Nano-TiO_2

R. Vinu and Giridhar Madras

Abstract This review discusses the utilization of photocatalysis for the degradation of water pollutants. Emphasis is placed on TiO_2 nanoparticles as a benchmark photocatalyst for the destruction of microorganisms and the degradation of a wide variety of organic compounds like phenolics, dyes, pesticides and pharmaceuticals. The mechanism of photocatalytic degradation is elucidated, underlining the importance of reaction kinetics for the efficient design of the processes. The effects of different reaction parameters on photocatalytic degradation are discussed. Surface modification of TiO_2 for visible light response by doping and heterostructuring is outlined. Finally, the challenges in the implementation of this technology for "real" waste water systems are summarized with a few attainable goals.

1 Introduction

The industrial revolution has led to the pollution of the natural resources in massive proportions. Environmental pollution caused by anthropogenic sources is a day-to-day problem faced by both developing and developed countries. Among the different types of pollution, air and water pollution from the point sources contribute a major share of the overall imbalance of the ecosystem. Common pollutants are usually toxic organic compounds like chlorinated and non-chlorinated aliphatic and aromatic compounds, dyes, detergents and surfactants, agro

R. Vinu · G. Madras (✉)
Department of Chemical Engineering, Indian Institute of Science,
Bangalore 560 012, India
e-mail: giridhar@chemeng.iisc.ernet.in

L. Zang (ed.), *Energy Efficiency and Renewable Energy Through Nanotechnology*,
Green Energy and Technology, DOI: 10.1007/978-0-85729-638-2_19,

wastes like insecticides, pesticides and herbicides, disinfection byproducts, volatile organic compounds, plastics, inorganic compounds (e.g., heavy metals), noxious gases (e.g., NO_x, SO_x, CO and NH_3) and pathogens (e.g., bacteria, fungi and viruses). Hence, strict environmental regulations on the use of these recalcitrant pollutants and their safe disposal drives the research community to develop clean and green processes to degrade the pollutants before they are discharged into the atmosphere and water bodies. This review examines "photocatalysis" as an advanced oxidation process for the degradation of different kinds of organic pollutants for environmental remediation.

Photolysis involves the use of ultraviolet (UV) or visible light radiation to effect chemical transformations. Photocatalysis uses a catalyst, usually, a semiconducting oxide to accelerate the photoreaction. The pioneering work of Fujishima and Honda in 1972 [1] on the photosplitting of water (i.e., simultaneous oxidation and reduction of water to oxygen and hydrogen, respectively) on a TiO_2 single crystal electrode led to the onset of photo induced redox reactions on semiconductor surfaces. This remarkable discovery attracted worldwide attention because it showed the possibility of generating hydrogen as a clean source of energy from water. It was soon realized that such redox processes could be utilized for environmental cleanup applications by Frank and Bard in 1977 [2], when they showed the photocatalytic oxidation of CN^- and SO_3^- using different semiconductor materials like TiO_2, ZnO, CdS, Fe_2O_3 and WO_3. This was followed by the demonstration of the TiO_2-catalyzed photodegradation of chlorinated organic compounds by Ollis [3, 4], and the Pt-loaded-TiO_2-catalyzed photochemical sterilization of microorganisms by Matsunaga et al. in the early 1980s [5]. Later, Grätzel, in 1991 [6], showed the first high-efficiency solar cell based on dye-sensitized colloidal TiO_2 films for photovoltaic power generation. Today, the principles of photocatalysis, especially using TiO_2 and its variants are widely employed in water and air purification, self-cleaning surfaces, self-sterilizing surfaces, antifogging surfaces, anticorrosive surface treatments, lithography, photochromic materials, microchemical systems and the selective and green synthesis of organic compounds.

Photocatalysis, as a research area, has witnessed tremendous development over the past two decades, with progress in the synthesis of novel materials and nanostructures, and the design of efficient processes for degradation of organic pollutants. Several classic review articles are dedicated to the principles and mechanism of photocatalysis [7–21], with special emphasis on the electron transfer processes, lattice and electronic structure of TiO_2, the surface chemistry of semiconductor oxides, generation of reactive radicals, chemisorption of small and large molecules, surface modification by doping and photooxidation of organic and inorganic substrates. Hence, photocatalysis can be regarded a well-understood field; yet, immense challenges and opportunities exist in realizing this technology on a large enough scale for pollution abatement.

Some of the traditional methods of water purification include neutralization of acidic and alkaline liquors, ultrafiltration, air stripping, flocculation, extraction, activated carbon adsorption, biological and peroxide/ozone treatment. It is

important to note that most of the above methods are non-destructive, i.e., they only transfer the pollutant to another phase and do not ensure its destruction. The peroxide/ozone (H_2O_2/O_3) treatment is an economical way to oxidize pollutants, but O_3 causes air pollution. Biological degradation methods are effective in reducing the biological oxygen demand of the effluent. However, achieving complete mineralization (i.e., complete conversion to CO_2 and H_2O) of the parent organic compound using the above methods is difficult. The potential of photocatalysis to accelerate the rate of degradation reactions is attributed to the generation of reactive hydroxyl radicals ($OH^{\bullet}$), which are the precursors of degradation of any organic or inorganic compound and microorganisms. These reactive species possess a higher oxidation potential (2.80 V) compared to other common oxidants like atomic oxygen (2.42 V), O_3 (2.07 V), H_2O_2 (1.78 V), hydroperoxy radicals (1.70 V) and chlorine dioxide (1.57 V) [15]. Moreover, the thrust to utilize solar radiation has made photocatalysis, the technology of choice for the detoxification of water pollutants.

This review article begins with an explanation of the basic principles of UV photocatalysis and the different semiconductor oxides, which are used as photocatalysts. Emphasis is on TiO_2 as a "benchmark photocatalyst", and the different synthesis procedures and properties of TiO_2 are briefly discussed. The photocatalytic degradation of various organic compounds like aliphatic and aromatic compounds, dyes, pesticides, pharmaceutical compounds and the destruction of microorganisms are extensively discussed in terms of their pathway of degradation. The effect of different reaction parameters like temperature, pH, solvents, UV light intensity, catalyst loading, substrate concentration, photocatalyst and the presence of anions and cations are discussed. The possibility of extending the absorption spectrum of UV photocatalysts to the visible region by appropriate surface modification is examined. The various mechanistic kinetic models proposed for the degradation of organic compounds are evaluated. The industrial applicability of photocatalysis is analyzed in the chemical engineering point of view, in terms of the different photoreactors that are currently being developed. Finally, the future research perspectives and the possibilities for commercializing this technology for the degradation of "real" industrial effluents are probed.

2 Mechanism of UV Photocatalysis

The mechanism of UV photocatalysis is well-documented [8, 10, 17, 18], and the following reactions represent the key steps in the generation of charge-carriers and hydroxyl radicals, which mediate photocatalytic reactions. A pictorial representation of the mechanism of TiO_2 photocatalysis is shown in Fig. 1.

Charge-carrier generation:

$$TiO_2 + h\nu \xrightarrow{h\nu > E_{BG}} h^+_{VB} + e^-_{CB} \quad (1)$$

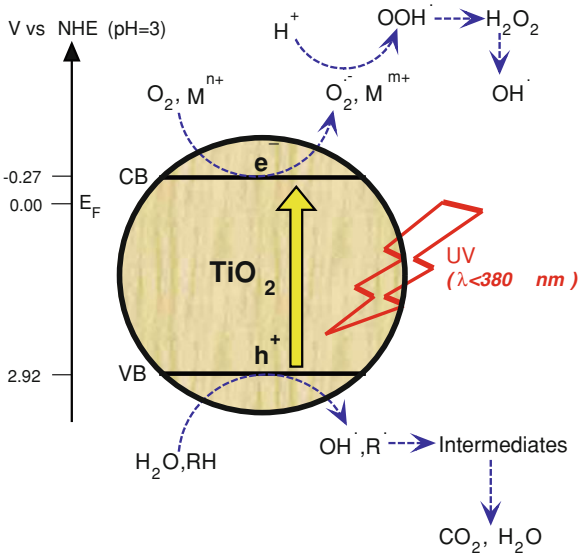

Fig. 1 Mechanism of photocatalysis on the surface of TiO_2 in presence of UV radiation

Charge-carrier trapping:

$$Ti^{IV}OH^- + h^+_{VB} \longrightarrow Ti^{IV} - OH^\bullet \tag{2}$$

$$Ti^{IV}OH^- + e^-_{CB} \rightleftharpoons Ti^{III} - OH^- \tag{3}$$

$$Ti^{IV} + e^-_{CB} \longrightarrow Ti^{III} \tag{4}$$

Electron–hole recombination:

$$Ti^{IV} - OH^\bullet + e^-_{CB} \longrightarrow Ti^{IV}OH^- \tag{5}$$

$$Ti^{III} + h^+_{VB} \longrightarrow Ti^{IV} \tag{6}$$

$$h^+_{VB} + e^-_{CB} \longrightarrow \text{heat} \tag{7}$$

Reactions in aqueous medium:

$$Ti^{IV} - H_2O + h^+_{VB} \longrightarrow Ti^{IV} - OH^\bullet + H^+ \tag{8}$$

$$Ti^{III} + O_2 \rightleftharpoons Ti^{III} - O_2^{-\bullet} \tag{9}$$

$$Ti^{IV} - O_2^{-\bullet} + 2H^+ + e^-_{CB} \rightleftharpoons Ti^{IV} - H_2O_2 \tag{10}$$

$$Ti^{IV} - O_2^{-\bullet} + H^+ \rightleftharpoons Ti^{IV} - HO_2^\bullet \tag{11}$$

$$Ti^{IV} - 2HO_2^\bullet \longrightarrow Ti^{IV} - H_2O_2 + O_2 \tag{12}$$

$$\mathrm{Ti^{IV} - H_2O_2 + e^-_{CB} \longrightarrow Ti^{IV} - OH^\bullet + OH^-} \quad (13)$$

$$\mathrm{Ti^{IV} - H_2O_2 + O_2^{-\bullet} \longrightarrow Ti^{IV} - OH^\bullet + OH^- + O_2} \quad (14)$$

Adsorption–desorption of a reductant (e.g., any organic substrate *S*):

$$\mathrm{Ti^{IV} + S \rightleftharpoons Ti^{IV} - S} \quad (15)$$

$$\mathrm{Ti^{IV} - OH^\bullet + S \rightleftharpoons Ti^{\mathit{IV}} - OH^\bullet - S} \quad (16)$$

Adsorption–desorption of an oxidant (e.g., metal ion)

$$\mathrm{Ti^{IV} + M^{n+} \rightleftharpoons Ti^{IV} - M^{n+}} \quad (17)$$

Photooxidation of a reductant:

$$\mathrm{Ti^{IV} - S + Ti^{IV} - OH^\bullet \longrightarrow Ti^{IV} + Ti^{IV} - \mathit{I} \longrightarrow CO_2 + H_2O} \quad (18)$$

$$\mathrm{Ti^{IV} - S + OH^\bullet \longrightarrow Ti^{IV} - \mathit{I} \longrightarrow CO_2 + H_2O} \quad (19)$$

$$\mathrm{Ti^{IV} - OH^\bullet - S \longrightarrow Ti^{IV} - \mathit{I} \longrightarrow CO_2 + H_2O} \quad (20)$$

$$\mathrm{Ti^{IV} - S + Ti^{IV}(h^+_{VB}) \longrightarrow Ti^{IV} + Ti^{IV} - \mathit{I} \longrightarrow CO_2 + H_2O} \quad (21)$$

Adsorption–desorption of the organic intermediate:

$$\mathrm{Ti^{IV} + \mathit{I} \rightleftharpoons Ti^{IV} - \mathit{I}} \quad (22)$$

Photoreduction of a metal ion:

$$\mathrm{Ti^{IV} - M^{n+} + me^- \longrightarrow Ti^{IV} - M^{(n-m)+}} \quad (23)$$

When TiO_2 or any semiconductor oxide is irradiated with UV light of energy greater than or equal to its bandgap (E_{BG}), valence band holes (h^+_{VB}) and conduction band electrons (e^-_{CB}) are produced (reaction 1). Hoffmann et al. [8] have found by laser flash photolysis studies that the characteristic time scale for this charge-carrier generation reaction is of the order of femtoseconds (fs). The charge carriers generated get trapped on the TiO_2 surface, which occurs over a time scale of tens of nano seconds (ns). Reaction 2 represents the trapping of the holes by the surface hydroxyl groups present in TiO_2, and reactions 3–4 represent the reversible trapping of the electrons on the surface of TiO_2 (shallow traps), and the irreversible trapping or relaxation of the electrons in the bottom of the conduction band (CB) (deep traps), respectively. Ti^{IV} denotes the four coordinated surface functionality of TiO_2 or the "active site". An important reaction that competes with the charge-carrier trapping is the electron–hole recombination reaction. As shown by reactions 5–7, electron–hole recombination can occur either at the surface states of the TiO_2, or in the bulk medium due to the delocalization of the electrons and holes from the surface. This is one of the most detrimental reactions in photocatalysis as this affects the interfacial charge transfer processes and hence the quantum

efficiency of the photoprocess. Hence, several techniques have been adopted to modify the semiconductor surface to increase the lifetime of the charge carriers by introducing surface trapping sites by the deposition of noble metals or transition metals. Due to the contact between the semiconductor and the metal, electrons flow from the CB of the semiconductor to the metal, until the Fermi levels of the two materials are aligned. This results in enhanced charge-carrier separation.

In an aqueous medium, valence band (VB) holes can react with the surface adsorbed water molecules to from hydroxyl species (reaction 8), and the trapped CB electrons can react with the dissolved oxygen in the system to form superoxide radicals (reaction 9). These superoxide radicals then undergo a series of reactions 10–14 with the solvated protons and the CB electrons to form hydrogen peroxide, hydroperoxy radicals, hydroxyl anions and hydroxyl radicals. Thus, hydroxyl radicals are generated by both the hole and electron pathways of photocatalysis. When the reactions are carried out in a non-aqueous (organic) medium, the surface bound hydroxyl species present in the semiconductor plays a major role (reaction 2), and the contribution of reactions 8–14 for the overall oxidation of the substrate is negligible.

The next reaction in the sequence is the adsorption of the target material (oxidant or reductant) onto the active sites of the photocatalyst. This is one of the crucial steps in heterogeneous photocatalysis as the reactions take place on the surface of the semiconductor photocatalyst. This is followed by the oxidation of the reductant and the concomitant reduction of the oxidant by the attack of hydroxyl radicals and CB electrons, respectively. The characteristic time scales for the above two processes are of the order of 100 ns and ms, respectively [8, 13]. This shows that the oxidizing powers of VB holes and hydroxyl radicals are always higher than that of the reducing power of the CB electrons. Moreover, these interfacial electron transfer steps compete with the electron–hole recombination reaction (10 ns), and hence, the practical efficiency or quantum yield is always lower than that of the theoretical yield. Reactions 18–21 denote the different possibilities by which the surface bound or solvated hydroxyl radicals and the VB holes can attack and degrade organic materials. Initially, organic intermediates are formed, which, on longer exposure to UV radiation, undergo mineralization to form CO_2 and H_2O. Once the reaction is complete, the unreacted reactants, intermediates and the products desorb from the surface of the catalyst (reactions 15–17, 22). Similarly, when metal ions are present in the system, they are reduced to their thermodynamically stable oxidation states by the CB electrons (reaction 23). This opens up a possibility to reduce the metal ions from their toxic to non-toxic states (e.g., Cr^{6+}–Cr^{3+}) by photocatalysis. Therefore, the overall photocatalysis reaction can be represented by reaction 24, wherein, the oxidants are reduced and the reductants are oxidized by the action of UV radiation on the semiconductor photocatalyst.

$$(Ox_1)_{ads} + (Red_2)_{ads} \xrightarrow{hv/TiO_2} Red_1 + Ox_2 \tag{24}$$

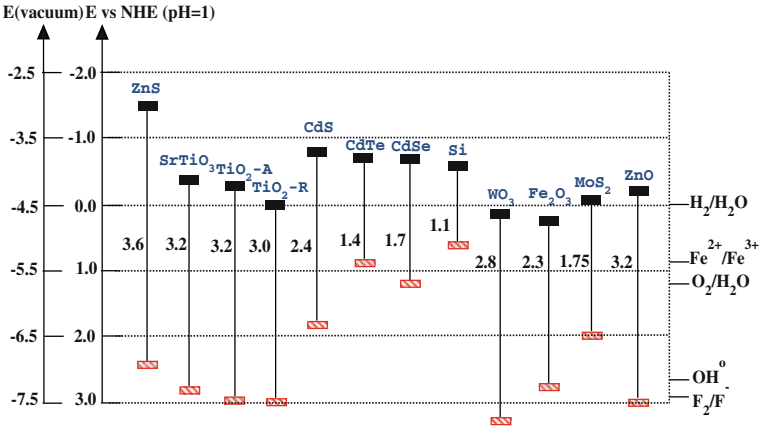

Fig. 2 Band gap energy and band edge positions of different semiconductor oxides and chalcogenides, along with selected redox potentials [12, 17, 22]

3 Semiconductor Photocatalytic Materials

Several metal oxides (TiO_2, ZnO, MoO_3, CeO_2, ZrO_2, WO_3, α-Fe_2O_3, SnO_2, $SrTiO_3$) and metal chalcogenides (ZnS, CdS, CdSe, WS_2, MoS_2) can be used as photocatalysts [10, 12, 17, 18]. However, energetics dictates that, for a semiconductor photocatalyst to be active, the redox potential of photogenerated VB holes must be sufficiently positive to generate hydroxyl radicals and that of CB electrons must be sufficiently negative to generate superoxide radicals. Figure 2 depicts the band structure diagram of the different materials, which have been tested for the photooxidation of organic compounds. It is clear that, TiO_2, ZnO, $SrTiO_3$ and CdS exhibit favorable bandgap positions compared to the other materials. The material selection is also based on the stability of the material toward photocorrosion. For example, ZnO and CdS have only one stable oxidation state (+2), and are prone to decomposition by VB holes. Furthermore, ZnO undergoes incongruous dissolution, yielding $Zn(OH)_2$ on the surface, thereby leading to the deactivation of the material over a period of time [18]. However, Ti in TiO_2 is capable of reversibly changing its oxidation state from +4 to +3; hence, TiO_2 is more favorable compared to the other materials. Between the two common crystal structures of TiO_2, viz., anatase and rutile—anatase phase TiO_2 is widely used in photocatalysis while rutile phase TiO_2 is used in pigments. Although rutile phase TiO_2 possesses a smaller band-gap energy (3.0 eV) compared to anatase phase (3.2 eV), indicating the possibility of the absorption of longer wavelength radiation, the former exhibits a higher photoactivity because of the position of the CB edge, which is more negative. This shows that TiO_2-anatase possesses a higher reduction power compared to that of TiO_2-rutile. In addition to the above advantages, other factors like its non-toxic nature (environmentally benign), low cost and the ease of synthesis makes TiO_2 the "photocatalyst of choice" for photocatalytic degradation reactions.

4 Synthesis and Properties of TiO_2

Different methodologies are being adopted for the synthesis of TiO_2. Many studies have concentrated on the synthesis of "nano-sized" TiO_2 for applications in photocatalysis. The importance of the nanometer regime stems from the fact that the physical, chemical, electrical and optical properties of the materials change immensely from the macroscopic to the nanoscale. One important property of nanoscale materials is the high surface to volume ratio of the material, which is beneficial to catalysis. This results in catalytic materials with high surface area and high porosity, which can promote high reaction rates owing to the high level of interaction of the reactants on the surface. Another important property is the efficient transport of the electrons and holes across the band gap of the material, which is governed by quantum confinement. The bandgap of the photocatalyst also dictates the wavelength at which the material can be excited. Hence, lower bandgap energies are beneficial for visible light absorption.

TiO_2 photocatalysts have been synthesized in different shapes and morphologies, which include, nanoparticles, nanorods, nanotubes, nanopillars and nanowire arrays, nanobowls, nanowhiskers, aerogels, nanosheets, opal and inversed opals [12, 14]. The synthesis routes can be broadly classified as solution phase and gas phase techniques. Solution phase synthesis is the most preferred technique for the preparation of TiO_2 in the form of powders and thin films. Some of the solution phase techniques are the precipitation method, hydrothermal synthesis, solvothermal synthesis, sol–gel method, sol method (nonhydrolytic sol–gel), micelle and inverse micelle method, combustion synthesis, electrochemical synthesis, sonochemical synthesis and microwave synthesis methodologies. Gas phase technique is widely employed for the synthesis of thin film samples. Some of the gas phase techniques are chemical vapor deposition (CVD), physical vapor deposition and spray pyrolysis deposition. Each of the above synthesis methods possesses a unique advantage over the other techniques, and the characteristics of the final product vary from one method to another. The review article by Chen and Mao [14] discusses each of the above synthesis techniques in detail, with particular emphasis on the morphology, size, shape and properties of the final TiO_2 product obtained in each method. Table 1 [23–30] presents a representative list of the different techniques adopted for the synthesis of TiO_2. These works elucidate that the final properties of TiO_2 nanoparticles like the phase composition (anatase : rutile), particle size, porosity, surface area, band gap and surface hydroxyl content can be tailored by varying the reaction conditions like: the precursor compound ($TiCl_4$, titanium(IV) isopropoxide, etc.), fuel (glycine, oxalyl dihydrazide, hexamethylene tetramine in the case of solution combustion synthesis), hydrolyzing agent (in the case of sol–gel synthesis), molar composition of the reactants, reaction temperature, reaction time (ageing time), calcination temperature and presence of gas atmosphere (air, Ar, NH_3).

One of the synthesis methodologies that has been proven to yield nano-TiO_2 with enhanced characteristics is the solution combustion method (CS TiO_2),

Table 1 Physicochemical properties of nano-TiO_2 by various synthesis techniques

Sl. No.	Synthesis method	Highlights/properties of TiO_2	Reference
1	Thermal decomposition of ammonium titanyl sulfate	Properties of TiO_2 tuned by varying the gas atmosphere and reaction temperature; mesoporous texture with mean pore dia. = 15 nm; particle size = 20–30 nm; surface area c.a. 64 $m^2\ g^{-1}$	[23]
2	Precipitation of a mixture of $Ti(OPr)_4$, stearic acid and 1-propanol, followed by calcination at different temperatures	Pore size tuned by adjusting the molar composition of stearic acid; pore dia. = 5–15 nm; surface area = 92–130 $m^2\ g^{-1}$	[24]
3	Four different synthesis routes involving the hydrolysis of $Ti(OPr)_4$ or $TiCl_4$ followed by calcination at different temperatures	Samples made from $TiCl_4$ exhibited the highest photoactivity; 100% anatase phase TiO_2 was obtained with crystallite size = 7–30 nm; surface area = 100 $m^2\ g^{-1}$; pore size = 7–14 nm	[25]
4	Combustion of aqueous titanyl nitrate with stoichiometric amounts of glycine at 350°C; precursor—$Ti(OPr)_4$	100% anatase phase TiO_2 was obtained; particle size = 8 ± 2 nm; band gap = 2.21 and 2.85 eV; surface area = 240 $m^2\ g^{-1}$; TGA wt. loss = 15.5%; high surface acidity	[26]
5	Hydrothermal synthesis using $TiCl_4$ using cationic surfactants like CTAB and CPB	Crystallite size = 10–18 nm; morphology change—nano-spheres to cotton fibrils; surface area = 240–418 $m^2\ g^{-1}$; pore size = 2–4 nm; mixture of anatase and rutile phase was obtained	[27]
6	Sol–gel synthesis using $Ti(OPr)_4$	Max. surface area = 125 $m^2\ g^{-1}$; min. crystallite size = 6 nm; band gap = 3.2±0.1 eV; mixture of anatase and rutile phase was obtained	[28]
7	One-pot hydrothermal synthesis using tetramethylammonium hydroxide (TMAOH)	Anatase phase TiO_2 nano-pillar arrays; c.a. 250 nm in width and c.a. 700 nm in length with a tetrahedral bipyramidal tip; optimum conditions—1M TMAOH, 200°C, 8 h	[29]
8	Combustion of aqueous titanyl nitrate with stoichiometric amounts of glycine at 350°C; precursor – $Ti(OBu)_4$	100% anatase phase TiO_2 was obtained; crystallite size = 4–6 nm; surface area = 257 $m^2\ g^{-1}$; band gap = 2.92 eV	[30]

$Ti(OPr)_4$—titanium(IV)isopropoxide; $Ti(OPr)_4$—titanium(IV)isobutoxide; CTAB—cetyltrimethylammonium bromide; CPB—cetylpyridinium bromide

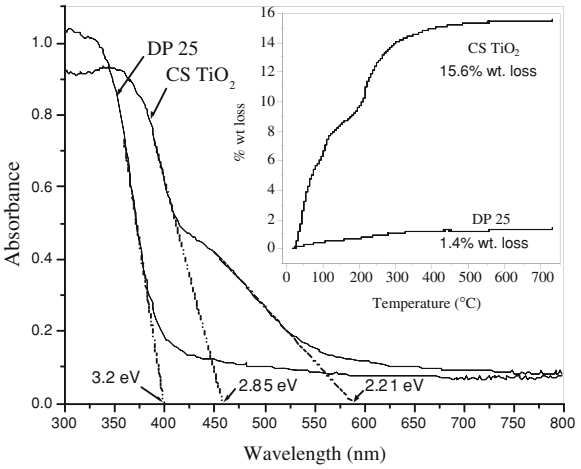

Fig. 3 UV/visible absorption spectra of CS TiO_2 and DP-25. The band gap values corresponding to the absorption threshold are shown. Inset: TGA thermograms [26]

developed by Nagaveni et al. [26]. CS TiO_2 exists in anatase phase, possesses a smaller particle size, higher surface area, lower band gap, higher amount of surface hydroxyl species and a highly acidic surface compared to the commercial P-25 TiO_2 (DP-25) produced by Degussa corporation. Figure 3 shows the UV/visible spectra and thermogravimetric analysis of CS TiO_2 and DP-25. It is clear that CS TiO_2 exhibits strong absorption in the visible region due to the carbide ion substitution for oxide ion, of the form $TiO_{2-2x}C_xV_x$, where 'V' denotes the oxide ion vacancy. Moreover, CS TiO_2 exhibits a higher weight loss compared to DP-25, indicating the presence of higher amount of surface hydroxyl groups. Table 2 [26, 31–35] compares the characteristics of CS TiO_2 with the other commercially available TiO_2 samples. It is evident that the activity of the photocatalyst cannot be standardized based on any single property, but by striking a balance between the different physicochemical properties. In a series of publications it was shown that the photoactivity of CS TiO_2 toward the photooxidation of different class of dyes [36–38], phenolic compounds like chlorophenols, nitrophenols and multiple substituted phenols [39, 40], substituted nitrobenzenes [41], water soluble polymers and plastics [42, 43] and the reduction of metal ions [44], is much higher compared to that of DP-25. More detailed discussions on the degradation of the organic compounds are available in later sections.

5 UV Photocatalytic Degradation of Organic Compounds

Chlorinated organic compounds like chloroalkanes were the first organic compounds to be degraded by photocatalysis [3, 4, 45]. Besides being widely used as solvents, pesticides, refrigerants and in plasticizers and plastics, these organochlorine compounds are toxic and accumulate in the environment. Hsiao et al. [3], and Pruden and Ollis [4] demonstrated complete mineralization of dichloromethane

Table 2 Comparison of the physicochemical properties of combustion synthesized TiO_2 (CS TiO_2) with commercially available TiO_2 samples

TiO_2	BET surface area, $m^2\ g^{-1}$	Crystallite size, nm	pH_{zpc}	Surface hydroxyl content	Reference
CS TiO_2	150	8±2 nm	2.4	15.6% total wt. loss (TGA)	[26]
DP-25 (80% A: 20% R)	50	A—37; R—90	6.3	1.4% (TGA); 163 (FTIR)	[26, 31]
Hombicat UV 100	290	5	6.0	843 (FT-IR)	[32, 33]
Junsei	9.7	34	4.4	52 (FT-IR)	[32]
Aldrich Anatase	9.2	37	4.2	54 (FT-IR)	[32]
Millenium PC 10	11	75	–	–	[34]
Millenium PC 50	50	25	–	–	[34]
Millenium PC 100	89.6	21	5.9	505 (FT-IR)	[32, 34]
Millenium PC 500	287	5–10	6.2	–	[34]
Tronox A-K-1	90	20	–	–	[35]
Ishihara ST-01	340	11	5.8	719 (FT-IR)	[32]

A—anatase; R—rutile; unless otherwise mentioned all the TiO_2 samples are 100% A

(CH_2Cl_2), chloroform ($CHCl_3$), carbon tetrachloride (CCl_4) and trichloroethylene in the presence of TiO_2, to HCl and CO_2. They observed that the chloride ions generated during the reaction act as inhibitors for the conversion of chloroalkanes. A Langmuir–Hinshelwood kinetic model was proposed to find the adsorption and degradation rate coefficients of the chloroalkanes and the chloride ions. The relative order of degradation of the chloromethanes is: $CHCl_3 > CH_2Cl_2 > CCl_4$.

A general stoichiometric reaction for the photocatalytic degradation of any organochlorine compound can be written as [8]:

$$C_xH_yCl_z + \left(x + \frac{y-z}{4}\right)O_2 \xrightarrow{h\nu,TiO_2} xCO_2 + zHCl + \left(\frac{y-z}{2}\right)H_2O \qquad (25)$$

Many studies have been devoted to the photocatalytic degradation of chlorinated aromatic compounds like chlorophenols and chlorobenzenes, chlorinated pesticides like DDT, hexachlorobenzene, atrazine and parathion, surfactants like sodium dodecyl benzene sulfonate and trimethyl phosphate, aliphatic and olefinic compounds, dyes, nitrogeneous compounds like nitrophenols and nitrobenzenes, carboxylic acids, alcohols and heteroatom compounds. The review articles by Hoffmann et al. [8], Mills and Hunte [10], Legrini et al. [15], Bhatkhande et al. [17] and Blake [46] have discussed the different studies on the photocatalytic degradation of different classes of organic compounds.

Although many organic compounds have been shown to photocatalytically degrade in presence of TiO_2, the mechanism of degradation of phenolic compounds like phenol, chlorophenols, nitrophenols and other substituted phenols, which are used as intermediates in the manufacturing of pesticides and herbicides,

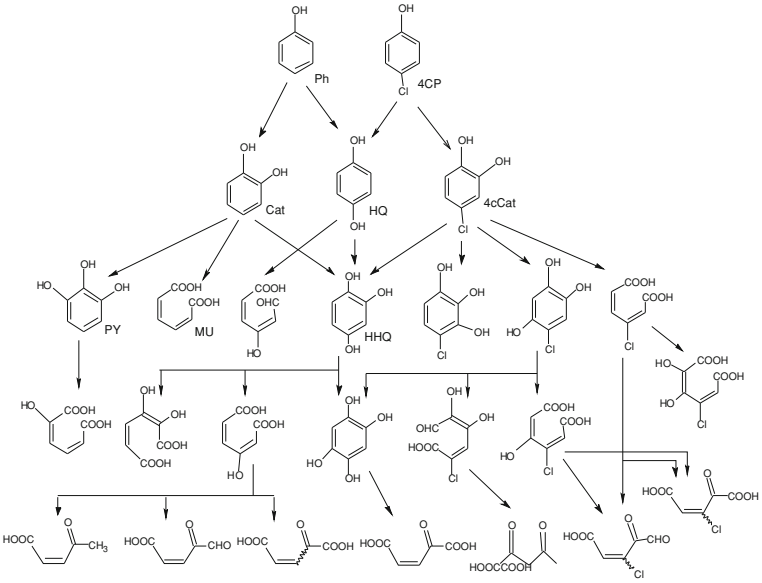

Fig. 4 Detailed pathway of degradation of phenol and 4-chlorophenol adapted from different studies. Some of the primary and secondary intermediates are identified as Ph—phenol, 4CP—4-chlorophenol, Cat—catechol, HQ—hydroquinone, 4cCat—4-chlorocatechol, PY—pyrogallol, MU—muconic acid and HHQ—hydroxyl hydroquinone [39, 47]

is well understood and documented. The degradation proceeds primarily by the attack of the hydroxyl radicals, which results in the hydroxylation of the parent compound at the ortho and para-positions, due to the ortho and para-directing nature of the phenolic –OH moiety. These are the primary intermediates, which, upon further exposure, results in the formation of a fully hydroxylated secondary intermediate species. The next step is the fragmentation of the benzene ring to form C-6 and C-5 aliphatic carboxylic acids and aldehydes.

In the case of chloro or nitro-substituted phenols, the hydroxyl group replaces the substituent group before the ring fragmentation. The longer (C-6, C-5, C-4) chain organic acids and aldehydes on longer exposure periods yield C-3, C-2 and C-1 organic acids. Finally, these shorter chain compounds mineralize to form CO_2 and H_2O. Li et al. [47] elucidated the mechanism of formation of the intermediates during the photocatalytic degradation of 4-chlorophenol and 4-chlorocatechol. Figure 4 shows the degradation pathway of phenol and 4-chlorophenol, adapted from different studies [39, 40, 47]. The photocatalytic degradation of phenol and 4-chlorophenol yields catechol, hydroquinone and chlorocatechol as the primary hydroxylated intermediates. Further hydroxylation steps result in the formation of pyrogallol, hydroxy hydroquinone and 4-chloro dihydroxy phenols. This step is followed by the fragmentation of the dihydroxy phenols to form muconic acid and muconic aldehydes with chloro and hydroxy-substitutions. A detailed mechanism of scission of the benzene ring is depicted in Figure 5. Muconic acid further

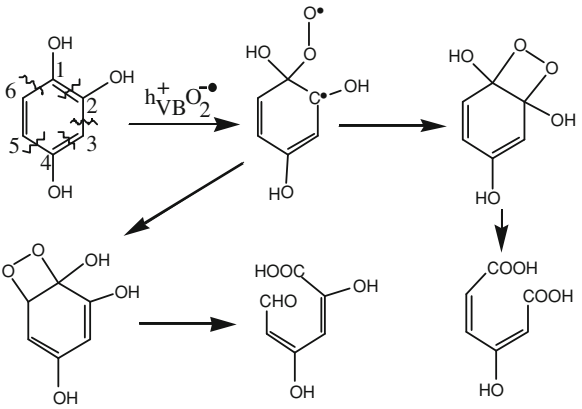

Fig. 5 Mechanism of cleavage of benzene ring in hydroxy hydroquinone, resulting in the formation of carboxylic acids and aldehydes. The possible sites of ring cleavage are represented by broken lines [47]

degrades to smaller organic acids like oxalic acid, maleic acid, succinic acid, fumaric acid, acrylic acid, etc. Finally, these acids mineralize to CO_2 and H_2O after long exposure periods.

Sivalingam et al. [39] studied the effects of different substituents like chloro group, nitro group and methyl group on the kinetics of photocatalytic degradation of phenol, and concluded that the order of degradation is: pentachlorophenol > trichlorophenol > dichlorophenol > 4-chlorophenol ≈ 2-chlorophenol > 2-methyl phenol ≈ 3-methyl phenol > phenol. Similarly, Priya and Madras [40] conducted a thorough study on the effect of multiple substitutions of the above groups on the degradation of phenol. Their results indicate that chloro-methylphenols (cresols) degraded much faster compared to chloro-nitrophenols, which was attributed to the ring deactivating nature of the nitro group for the hydroxyl radicals to react with the phenolic compound. Another interesting conclusion of their study shows that the degradation is independent of the position of the substituents, but depends on the nature of the substituent group. In another study [41], it was found that chloro and hydroxy-substitution in nitrobenzene accelerated the degradation rate, while nitro-substitution resulted in a reduced degradation rate of nitrobenzene.

Other important organic compounds, which have attracted interest in the past decade, include dyes, pesticides and pharmaceutical compounds. The forthcoming sections will examine the various studies on the photocatalytic degradation of these pollutants.

5.1 Dyes

Dyes constitute a major class of organic compounds, which find a multitude of applications in our daily life in clothing, food, paper, leather, cosmetics, plastics, drugs, electronics and printing. The modern textile industry consumes about 80% of all synthetic dyes produced, with 700,000 tons of dyes applied to 40 million tons

of fabric annually [48]. One of the major bottlenecks in the textile industry is dye fixation (i.e., spent dye baths, residual dye liquors and water from washing operations contain dye in the hydrolyzed and unfixed form). Although dye fixation depends on the class of the dye, type of fabric and other dyeing parameters, nearly 10% of the dyes used are discharged into the effluent as a result of this process. Hence, reducing the toxicity levels to permissible limits before admitting the dye waste water to aquatic bodies is a critical issue. In this regard, photocatalysis, as an AOP, has played a significant role in the degradation of textile dye effluents. Many reviews exclusively discuss the degradation of different classes of dyes under UV and visible light exposure [48–50], various parameters affecting the degradation of dyes [51], and modified TiO_2 materials for the degradation of dyes [52].

Based on the functional group that constitutes the dye molecules, dyes can be classified as azoic, anthraquinonic, heteropolyaromatic, aryl methane, xanthene, indigo, acridine, nitro, nitroso, cyanine and stilbene. Among all the above dye functionalities, photodegradation of azo dyes has been investigated extensively [50], as these dyes contribute 50% of the commercial dyes. The degradation of a dye can be characterized in two ways: percent decolorization and percent mineralization. Decolorization refers to the reduction in concentration of the parent dye molecule under consideration at its characteristic wavelength, but does not refer to the complete removal of the organic carbon content. This is due to the formation of colored dye intermediates, which might absorb at a different wavelength. Hence, complete degradation or mineralization occurs when all the organic carbon is converted to CO_2. Therefore, analyzing the mineralization of the dyes in terms of the total organic carbon (TOC) content assumes importance. The mechanism of CO_2 evolution from an organic dye intermediate is well-documented and it follows the photo-Kolbe decarboxylation mechanism [53]. The reaction is given by:

$$\Phi - \mathrm{COO}^- + h^+_{\mathrm{VB}} \longrightarrow \Phi^\bullet + \mathrm{CO}_2 \tag{26}$$

In Eq. 26, Φ denotes the organic component of the dye or the dye intermediate. The radical $\Phi^\bullet$ formed as a result of this reaction can undergo further transformation to yield other intermediates with smaller sizes.

Epling and Lin [54] degraded 15 dyes belonging to different classes of functionality in the presence of visible light. Their results show that the presence of electron withdrawing groups retards the degradation of the dye. The order of degradation among the different dyes follows this order: indigo $\approx$ phenanthrene $>$ triphenyl methane $>$ azo $\approx$ quinoline $>$ xanthenes $\approx$ thiazine $>$ anthraquinone. Moreover, the order of degradation of the dyes in the presence of different light sources follows: natural sunlight $\gg$90 W halogen flood light $>$150 W spotlight. They have attributed the degradation of the dye to both photosensitized oxidation and reduction mechanisms.

Vinu et al. [38] studied the degradation of 5 anionic, 8 cationic and 3 solvent dyes, each belonging to a different class by molecular structure, with CS TiO_2 and DP-25 in the presence of UV irradiation. It was observed that the order of

degradation of the dyes with CS TiO_2 and DP-25 was different, and this was correlated to the surface charge of the catalysts. By monitoring the shift in the characteristic wavelength of the dyes during degradation, it was concluded that the formation and consumption rates of the intermediates were high in the presence of highly acidic surface of CS TiO_2, while significant amounts of intermediates were observed in the presence of DP-25. Overall, anionic dyes exhibited higher decolorization rates compared to the cationic dyes, and the solvent dyes exhibited adsorption dependent degradation.

Silva et al. [55] studied the degradation of mono, di and tri-azo dyes and found that the decolorization followed the order: Solophenyl Green BLE (tri-azo) > Erionyl Red B (di-azo) > Chromotrop 2R (mono-azo). However, the mineralization of the dyes followed the opposite trend. All the above studies suggest that a correlation does not exist between the degradation rate of the dye with the dye structure or the functional groups that characterize the dye. Therefore, it is important to analyze the pathway of degradation of the dyes in order to assess the stability of the different intermediates.

A representative list of the studies devoted to the analysis of the organic intermediates during the degradation of the dyes is presented in Table 3 [53, 56–63]. Rajeshwar et al. [48] provided an extensive list of the studies on the degradation pathway of azo and non-azo dyes. A generalized conclusion is that alkyl substituted (methyl or ethyl) dyes like triphenyl methane or rhodamine dyes degrade by the N-de-alkylation mechanism, which involves the abstraction of the alkyl groups by the hydroxyl radicals resulting in the formation of the corresponding aldehyde as a side product. Once complete dealkylation occurs, fragmentation of the molecule occurs, which results in the formation of different substituted benzene compounds. At long exposure periods, the cleavage of benzene ring results in the formation of low molecular weight organic acids. The degradation of azo dyes involves the cleavage in the vicinity of the azo bond and results in the formation of naphthol and benzoic acid intermediates. Likewise, the degradation pathway of anthraquinone dyes result in the formation of phthalic acid intermediates.

The dye molecules also contain other hetero atoms like N, S, Br and Cl in their structure, and hence, an assessment of the fate of these elements during mineralization is also critical. It has been well established that sulfonate groups ($–SO_3^-$) in anionic dyes are transformed to innocuous sulfate ions (SO_4^{2-}), primary ($–NH_2$) and secondary (–NH–) amino groups are converted into ammonium ions (NH_4^+), azo nitrogen (–N=N–) is converted to N_2 and halogen atoms are released into the solution as their respective anions. The following reactions describe the mechanism by which the above transformations take place [53]:

Formation of sulfate ions:

$$\Phi - SO_3^- + OH^\bullet \rightarrow \Phi - OH + SO_3^{\bullet -} \tag{27}$$

$$SO_3^{\bullet -} + OH^- \rightarrow H^\bullet + SO_4^{2-} \tag{28}$$

Table 3 Survey of the organic intermediates formed during the photocatalytic degradation of different classes of dyes

Sl. No.	Dye/dye category	Organic intermediates detected	Reference
1	Acid Orange 7/mono-azo	22 intermediates were detected; coumarin, 2-maphthol, naphthoquinone derivatives, phthalic acid, phthalic acid, phthalimide, benzoic acid derivatives, phenol, succinic acid, maleic acid, malonic acid, etc.	[56]
2	Metanil Yellow/Mono-azo	Benzenesulfonic acid, hydroxylated diphenyl amine, diphenyl amine, benzene, aniline, phenol, hydroquinone	[57]
3	Procion Red MX-5B/ Triazine+mono-azo	12 intermediates were detected; *p*-hydroxy-phenyl-3-hydroxy propanedioic acid, 2-hydroxy benzoic acid, *p*-hydroxy cinnamic acid, phthalic acid, malic acid, oxalic acid, etc.	[58]
4	Remazol Brilliant Blue R/Anthraquinonic	Amino and hydroxyl substituted anthraquinone, phthalic acid, amino substituted phthalic acid	[59]
5	Indigo and Indigo Carmine/Indigo	2-Nitro benzaldehyde, 2,3-dihydroxy indoline, anthranilic acid, tartaric acid, malic acid, amino-fumaric acid, pyruvic acid, malonic acid, glycolic acid, oxalic acid, acrylic acid, acetic acid, etc.	[60]
6	Methylene Blue/ Heteropolyaromatic	(3-dimethyl amino) aniline, benzene sulfonic acid, phenol, hydroxylation of amino and sulfoxide groups was observed	[53]
7	Rhodamine B/Xanthene fluorene	Mono-, di-, tri- and tetra-*N*-de-ethylated rhodamine species, rhodamine 110	[61, 62]
8	Methyl Green/Triphenyl methane	33 intermediates were identified and characterized; major intermediates—colorless carbinol base and crystal violet dye; degradation proceeded by *N*-de-methylation and *N*-de-alkylation pathway; methylated and ethylated derivatives of aminophenol and benzophenone were observed	[63]

Formation of ammonium ion:

$$\Phi - \mathrm{NH} - \Phi' + \mathrm{H}^{\bullet} \rightarrow \Phi^{\bullet} + \Phi' - \mathrm{NH_2} \tag{29}$$

$$\Phi' - \mathrm{NH_2} + \mathrm{H}^{\bullet} \rightarrow \Phi'^{\bullet} + \mathrm{NH_3} \tag{30}$$

$$\mathrm{NH_3} + \mathrm{H}^{+} \rightarrow \mathrm{NH_4^{+}} \tag{31}$$

Formation of N_2:

$$\Phi - \mathrm{N} = \mathrm{N} - \Phi' + \mathrm{H}^{\bullet} \rightarrow \Phi - \mathrm{N} = \mathrm{N}^{\bullet} + \Phi' - \mathrm{H} \tag{32}$$

$$\Phi - \mathrm{N} = \mathrm{N}^{\bullet} \rightarrow \Phi^{\bullet} + \mathrm{N} \equiv \mathrm{N} \tag{33}$$

Formation of chloride/bromide ions:

$$\Phi - Cl/Br + OH^{\bullet} \rightarrow \Phi - OH + Cl^{-}/Br^{-} \quad (34)$$

5.2 Pesticides

Pesticides encompass a class of organic compounds used for preventing, destroying or controlling pests. These are widely applied on agricultural crops to protect them from insects, pathogens, weeds, moths, microbes, etc. However, the continuous usage of pesticides results in poor soil quality, reduced nitrogen fixation for plants and poisoned food sources. Also serious is the transfer of these compounds to water bodies by leaching, percolation, spillage or runoff, which poses ill-effects to human health and other forms of life. Based on the chemical structure, pesticides can be classified as organochlorine compounds, organophosphorous compounds and carbamate compounds, which contain nitrogen, phosphorous, sulfur, chlorine and heterocyclic nitrogen atoms. Therefore, the mineralization of pesticides should result in the conversion of these hazardous compounds to innocuous products of N, S and P, along with CO_2 and H_2O.

A variety of pesticides like atrazine (s-triazine) [64], propanil (acetanilide) [64], molinate (thiocarbamate) [64], pyridaben [65], methamidophos [66], methyl parathion [67], cyproconazole [68], hexachloro benzene [69], dicofol [69], pyrimethanil (fungicide) [70], primicarb (insecticide) [70], propyzamide (herbicide) [70], etc., have been photocatalytically degraded using TiO_2. Many studies have proposed a detailed pathway of degradation of the pesticides by monitoring the formation of intermediates by HPLC/MS/MS and GC/MS techniques. It was found that, during mineralization, phosphorous is converted to orthophosphoric acid (H_3PO_4), nitrogen to NO_3^- and NH_4^+ ions and sulphur to SO_4^{2-} ions. Figure 6 depicts the pathway of degradation of triazophos, an organophosphorous pesticide [71].

5.3 Pharmaceutical Compounds

Recently, photocatalytic degradation of pharmaceutical compounds and drugs has received attention, as these compounds are found in the effluents in levels ranging from ng L^{-1}–μg L^{-1}. These compounds are admitted into waste water and aquatic bodies by manufacturing operations, spillage, human and animal excretion and hospital wastes. Besides leading to serious hazards like genotoxicity, endocrine disruption and aquatic toxicity, these xenobiotic substances increase the resistance of the pathogenic bacteria in waste water. These compounds are resistant toward biological degradation and other common oxidation techniques, and thus, build up their concentration in the ecosystem. In fact, clofibric acid, which is used as a

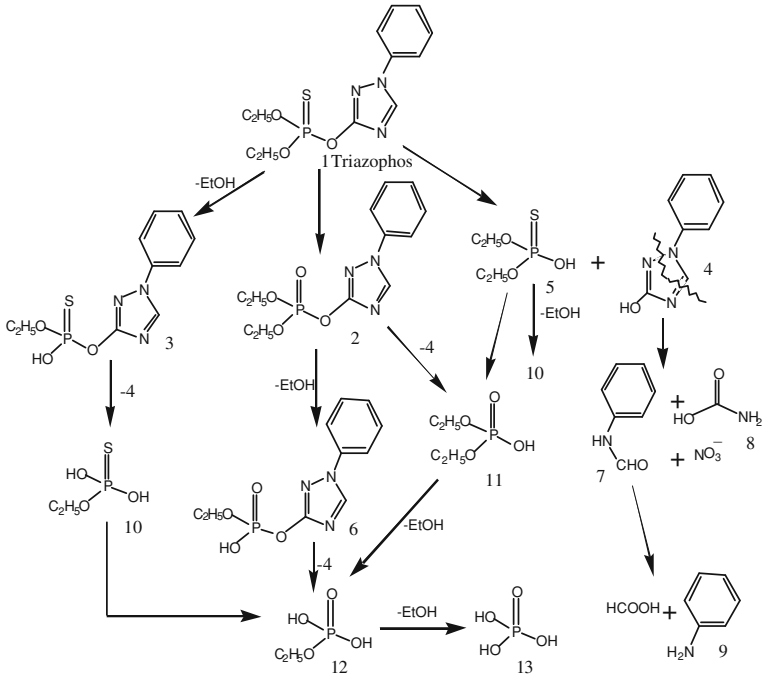

Fig. 6 Pathway of degradation of the pesticide, triazophos, established using LC/MS/MS and GC/MS/MS [71]

regulator of lipids in the blood, is still detected in lakes and rivers, even after 21 years of persistence in the environment [72]. Therefore, photocatalysis has emerged as an alternative for the effective degradation and mineralization of these persistent organic pollutants.

The different pharmaceutical compounds that were subjected to photocatalytic degradation using TiO_2 are listed in Table 4 [72–79]. The degradation of a wide class of compounds has been studied, and many studies have optimized the reaction parameters like pH, O_2 concentration and TiO_2 loading for maximum conversion of the parent drug compound. Most of these studies have also established the pathway of degradation of the pharmaceutical compounds, by following the evolution of the intermediates via mass spectroscopy. A generalized conclusion in each of the above studies is that the time taken for the complete mineralization of the pharmaceutical compound was longer compared to the removal of the parent compound. Calza et al. [80] studied the photocatalytic degradation and ecotoxicity of amiloride, a diuretic agent, and concluded that although amiloride is non-toxic, the degradation intermediates were toxic compounds. Similar results were also observed for salbutamol [79], indicating the importance of complete mineralization of the drug to CO_2, H_2O and inorganic ions. Figure 7 depicts the pathway of degradation of diclofenac, a non-steroidal anti-inflammatory drug [78].

Table 4 Listing of recent studies on the photocatalytic degradation of different pharmaceutical compounds

Sl. No.	Compound class	Pharmaceutical compounds
1	Antibiotic	Chloramphenicol [73], sulfamethoxazole [74], ciprofloxacin [75], ofloxacin [72]
2	Analgesic and antipyretic	Paracetamol [76], phenazone [72]
3	Non-steroidal anti-inflammatory drug (NSAID)	Diclofenac [77, 78], naproxen [77], ibuprofen [77]
4	Beta blocker	Atenolol [76]
5	Anti convulsant	Carbamzepine [72]
6	Anti cholestric	Clofibric acid [72]
7	Histamine H_2—receptor antagonist	Ranitidine hydrochloride [72]
8	Loop diuretic	Furosemide [72]
9	Beta 2-agonist	Salbutamol [79]

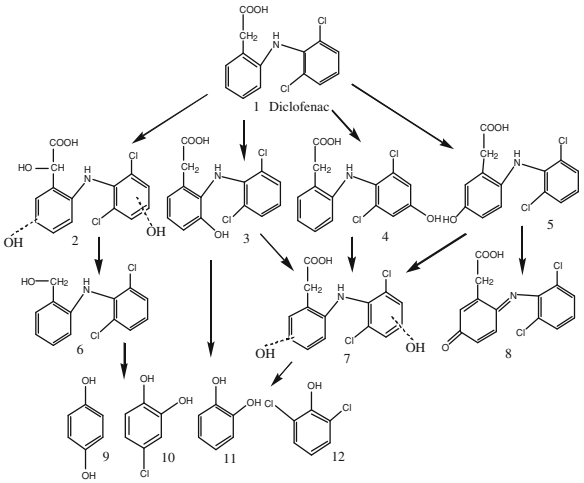

Fig. 7 Degradation pathway of the non-steroidal anti-inflammatory drug, diclofenac, established using ESI–MS. The dotted lines in the compounds 2 and 7 shows that the hydroxyl radicals can attack either of the benzene rings to form the intermediate [78]

6 Photocatalytic Destruction of Microorganisms

Microorganisms like pathogenic bacteria, fungi, viruses and protozoa in drinking water and air pose a severe threat to human and animal life; they are the primary carriers of infectious diseases like gastroenteritis, cholera, tuberculosis, anthrax, malaria and yellow fever. Conventional disinfection technologies employ chlorine, chlorine dioxide (ClO_2), hypochlorite (OCl^-) or ozone as disinfectants, owing to their low operating cost and applicability in a wide pH range. However, the byproducts of the above techniques involve the formation of halomethanes and halo acetic acids, which are carcinogenic even at low concentrations. Hence, photolytic (UV-C radiation at 254 nm) and photocatalytic disinfection

(UV-A at 365 nm or visible radiation) of microorganisms, using TiO_2 as the photocatalyst has been researched extensively for the past two decades. Table 5 [81–90] shows the different studies devoted to the deactivation of various kinds of microorganisms using different semiconductor materials. Among the different microorganisms, *Escherichia coli* (*E. coli*), a Gram negative rod shaped bacterium, owing to its presence in the intestines of humans, animals and birds, serves as a biological indicator to test environmental samples for fecal contamination. Unlike organic compounds, the concentration of microorganisms is usually expressed in terms of the number of colony forming units per mL of the solution (cfu mL^{-1}). CFU refers to the number of viable microbial colonies, which are measured by counting the cell aggregates on an agar plate.

Cho et al. [91] evaluated the inactivation of *E. coli* under different light intensities, TiO_2 concentration and pH, and have observed a linear correlation of the inactivation time (for 2-log reduction) with the hydroxyl radical concentration in the system. This study suggests that hydroxyl radicals are more important than the reactive oxygen species, and that they are 1000–10000 times as effective as common oxidants like chlorine, chlorine dioxide or ozone for the disinfection of *E. coli*. The mechanism of photocatalytic disinfection of microorganisms is different from that of the degradation and mineralization of organic compounds, although the hydroxyl radicals are the precursors of degradation in both the cases. The primary reason concerning the complex nature of inactivation of microorganisms is due to their large size and complex structure compared to organic molecules. This results in several pathways of cell rupture and regeneration.

Many modes of cell wall damage of the microorganisms have been proposed. Matsunaga et al. [92] observed a decrease in Coenzyme A (CoA) content in the cell and a concomitant increase in concentration of the dimeric form of CoA, when *E. coli* was irradiated in presence of TiO_2. Since the electron transfer between the cell and the TiO_2 is mediated by CoA, the reduction in its concentration was attributed to cell damage. Saito et al. [93] observed a "rapid" leakage of potassium ions and the "slow" release of protein and RNA during the lysis of *Streptococcus sobrinus*, in presence of UV/TiO_2. Thus, they concluded that the inactivation is due to the loss of permeability of the cell wall of the bacteria. Maness et al. [94] have observed an exponential increase in the concentration of malondialdehyde during the inactivation of *E. coli*, suggesting that the active species like hydroxyl, hydroperoxy and superoxide radicals attack the polyunsaturated phospholipids in *E. coli*, which results in lipid peroxidation and hence the loss of respiratory activity of the cell.

Thus, it is unequivocally accepted that the cell wall damage induced by the active species in presence of UV/TiO_2 is the primary cause for the death of the microorganisms. However, it must be ensured that complete disinfection (99.999%) takes place and microorganisms are indeed in their inactive state, even after the irradiation and/or TiO_2 is removed from the system. This is because, the presence of active bacteria may result in their reproduction, as organic compounds like aldehydes, ketones and carboxylic acids, which are usually the products of cell damage, serve as nutrients for further growth. It has widely been observed that the

Table 5 Photocatalytic disinfection of microorganisms using TiO_2 in presence of UV and visible light radiation

Sl. No.	Microorganism	Concentration	Catalyst	Loading	Light source	Reference
	UV radiation					
1	*Legionella pneumophila*	10^7 cfu mL^{-1}	TiO_2	1 g L^{-1}	λ = 365 nm; I = 108 μW cm^{-2}	[81]
2	*E. coli, Pseudomonas aeruginosa, Salmonella typhimurium, Enterobacter cloacae*	10^6–10^7 cfu mL^{-1}	DP-25 TiO_2	0.1 g L^{-1}	λ = 365 nm; I = 5.5,1.4 mW cm^{-2}	[82]
3	*Bacillus anthracis*	700–1900 cfu mL^{-1}	TiO_2	10–100 mg	λ = 320–400 nm; I = 0.42–2.43 mW cm^{-2}	[83]
4	*E. coli, Lactobacillus helveticus*	10^8 cfu m L^{-1}	TiO_2 and ZnO	1,2 g L^{-1}	λ = 365 nm; I = 20 W m^{-2}	[84]
5	*E. coli*	10^9 cfu mL^{-1}	Ag impregnated TiO_2	2 g L^{-1}	λ = 280 nm; I = 0.5 W m^{-2}	[85]
6	*E. coli, Staphylococcus aureus*	5×10^7 cfu mL^{-1}	AgI/TiO_2	0.2 g L^{-1}	350 W XL; I = 2.8 mW cm^{-2}	[86]
7	*E. coli*	1 – 4×10^8 cfu mL^{-1}	Montmorillonite supported Ag/TiO_2	0.4 g L^{-1}	40 W FL	[87]
8	*E. coli, Pseudomonas aeruginosa, Staphylococcus aureus*	10^7 cfu mL^{-1}	PdO and N doped TiO_2	1 g L^{-1}	I = 0.4–1.6 mW cm^{-2}	[88]
9	*Micrococcus lylae*	3×10^7 cfu mL^{-1}	S doped TiO_2	0.2 g L^{-1}	100 W WHL; I = 47 mW cm^{-2}	[89]
10	*Microcystin-LR*	1 mg L^{-1}	N–F-codoped TiO_2		Two 15 W FL; I = 78 μW cm^{-2}	[90]

XL—xenon arc lamp; FL—fluorescent lamp; WHL—tungsten halogen lamp

inactivation rate of microorganisms in pure, deionized water is higher compared to that in the presence of tap water or water contaminated with ionic species or humic substances [95]. This is due to the osmotic stress in deionized water, which results in the easy leakage of potassium, calcium and magnesium ions through the cell membrane, thereby leading to the loss of permeability. Moreover, humic substances compete for the reactive radicals, which results in the inhibition of the disinfection rate.

From Table 5, it is clear that TiO_2 and its modified forms have shown superior photocatalytic activity for the disinfection of a wide class of Gram-positive and Gram-negative bacteria and other microorganisms in water, both in presence of UV and visible light irradiation. The initial concentration of the microorganisms that is widely used in the recent works corresponds to 10^3–10^9 cfu mL^{-1}. It is also interesting to note that the optimum catalyst concentration varies widely across the different studies, suggesting the strong dependence on the intensity of irradiation, with high intensities requiring lesser catalyst loading. Pal et al. [96] recently evaluated the disinfection of air borne *E. coli* in a continuous annular reactor in presence of TiO_2. Complete inactivation of *E. coli* was observed using UV-A irradiation of 3.4 mW cm^{-2} intensity, 85% relative humidity and 1516 mg m^{-2} of TiO_2, within a residence time of 1.1 min. Recently, Ag is incorporated into TiO_2, either on the surface or in the lattice, to enhance the biocidal activity of bare TiO_2 [85–87]. The advantages of having Ag as a component in the photocatalyst are three fold: (i) Ag^+ ions possess an inherent antimicrobial activity, which complements the disinfection ability of TiO_2, (ii) Ag, when impregnated on the surface of TiO_2, acts as electron trapping sites, which retards the unwanted charge-carrier recombination, (iii) nano-sized Ag promotes the formation of electrons in presence of visible radiation, due to the surface-plasmon excitation. These electrons are transferred to the conduction band of TiO_2, thereby leading to the formation of reactive superoxide radicals. However, it has been observed in a recent study that an optimum loading of 1% Ag onto TiO_2 yielded a maximum rate of disinfection of *E. coli* [85]. The synthesis of Ag nanoparticles and their incorporation onto different substrates by different techniques, and the anti-microbial activity are discussed elsewhere [97].

7 Effect of Reaction Conditions

7.1 Temperature

Minor incremental changes in temperature do not significantly affect the rate of photocatalytic reactions. However, higher temperatures might result in the reduction of dissolved oxygen in the solution. Dissolved oxygen is one of the key elements in photocatalysis, as it aids in scavenging CB electrons, thereby leading to the formation of hydroxyl radicals by the electron pathway. Moreover, higher temperatures result in desorption of the organic compounds from the surface of the

photocatalyst. Because photocatalytic degradation is a surface mediated phenomenon, desorption of the organic compound before the reaction results in a decrease in the reaction rate. Naeem et al. [98] studied TiO_2 photocatalyzed degradation of phenol, 4-chlorophenol and 4-nitrophenol in the temperature range 25–45°C and found that increasing the temperature does not significantly enhance the degradation rates. The apparent activation energy of photocatalytic degradation ranges from 9.68 to 21.44 kJ mol^{-1}, which is much lower than that of thermal degradation reactions (e.g., 66.5 kJ mol^{-1} for the thermal degradation of poly(α-methyl styrene) in solution [99]).

7.2 pH

Photocatalytic degradation reactions are highly sensitive to pH of the reaction mixture. This is due to the fact that the adsorption of the organic compound onto the photocatalyst surface, and, therefore, the degradation reaction depends on the surface charge of the photocatalyst and also on the ionization state of the organic compound. TiO_2 exists in the following protonated and deprotonated forms in acidic and basic medium, respectively [48].

Acidic medium:

$$> \mathrm{Ti} - \mathrm{OH} + \mathrm{H}^+ \rightleftharpoons > \mathrm{Ti} - \mathrm{OH}_2^+ \tag{35}$$

Basic medium:

$$> \mathrm{Ti} - \mathrm{OH} + \mathrm{OH}^- \rightleftharpoons > \mathrm{TiO}^- + \mathrm{H_2O} \tag{36}$$

Hence, the adsorption of positively charged organic compounds is facilitated at a basic pH, while that of negatively charged species is favorable at an acidic pH of the TiO_2 surface. In this regard, pH_{zpc}, the zero-point charge pH or the isoelectric pH of the TiO_2 photocatalyst plays a crucial role. At a $pH < pH_{zpc}$, the TiO_2 surface becomes positively charged (acidic), while at a $pH > pH_{zpc}$, it becomes negatively charged (basic). The effect of pH on the photocatalytic degradation of dyes was extensively reviewed by Konstantinous and Albanis [50], and Akpan and Hameed [51]. Sivalingam et al. [39] observed that dyes like Orange G (anionic) and Methyl Red (neutral) degrade at higher rates at low pH (4.1) values, while Congo Red (anionic) and Alizarin Red S (anionic) degrade at high pH (9.1) values. Devi et al. [100] investigated the degradation of anionic and cationic dyes in presence of Mo^{6+} ion-substituted TiO_2 under different pH's, and correlated the degradation behavior of the dyes with the adsorption tendency of the dye at different pH levels. They observed that the rate coefficients for the degradation of anionic dyes were higher at an acidic pH (5.6), while that of cationic dyes were higher at a basic pH (8.0). Therefore, it can be concluded that pH is a very complex parameter, which depends both on the surface charge of the photocatalyst and the nature of the organic compound, and hence, it is difficult to standardize the

pH conditions for the degradation of a specific class of organic compounds. However, for the inactivation of microorganisms, it was found that the disinfection rate is nearly the same in the pH range of 4–9. This was attributed to the acid-induced proteins in *E. coli* and *Salmonella typhimurium*, which impart acid tolerance to these cells [95, 101].

7.3 Wavelength and Intensity of the Light Source

The properties of the UV light source, viz., the wavelength and intensity, play a key role in the excitation of semiconductor photocatalyst and the generation of reactive radicals. Matthews and McEvoy [102] degraded phenol and salicylic acid in the presence of 254 nm (UV-C; germicidal lamp) and 350 nm (UV-A; black-light fluorescent lamp), and concluded that the photocatalytic degradation rate is higher in presence of 254 nm radiation. This is because of the high energy of the 254 nm photons (112.6 kcal Einstein^{-1}) compared to that of the 350 nm photons (81.7 kcal Einstein^{-1}). However, the thrust to realize photocatalytic degradation in the presence of sunlight or visible radiation has resulted in light sources operating at wavelengths 365 nm and above, preferable to the 254 nm high-energy radiation, which is filtered by the atmosphere.

The intensity of radiation is related to the photon energy flux and quantum yield of the photoprocess. Photon energy flux is defined as the number (or energy) of photons per second per unit area incident on the reaction mixture. It is expressed in terms of the intensity of the incident radiation (I_0), volume of the reaction mixture (V) and the area of the exposed solution (A) as $I_0 V N_A E_\lambda / A$, where N_A is Avagadro's number of photons per mole, and E_λ is the energy of the incident photon at wavelength λ. Photon flux is expressed in terms of W m^{-2} and is usually determined by chemical actinometric techniques [103]. Quantum yield, $\Phi(\lambda)$, is defined as the ratio of number of molecules undergoing chemical transformation to the number of photons absorbed in that period of time. As the number of photons absorbed depends on the input energy density of the photons, the intensity of the light source has a positive effect on the photocatalytic degradation rate of an organic compound. Ollis et al. [45] classified the variation of the reaction rate with intensity into three regimes. At low I_0, the degradation rate is linearly proportional to I_0; at intermediate I_0, the degradation rate is proportional to $I_0^{1/2}$, and at high I_0, the degradation rate is independent of I_0, due to mass transfer limitations. Meng et al. [104], by assuming that the total number of H_2O/OH^- in the system is insufficient to capture the holes, showed that, in the intensity range from 0.86 to 6.8 mW cm^{-2}, the adsorption and degradation rate constants signifying the degradation of p-chlorobenzoate vary with the intensity as $I^{-1/2}$ and $I^{1/2}$, respectively. Wu and Chern [105] used a first-order correlation of the form, $[h\nu] = I_0 \exp(-k[TiO_2])$, to account for the screening effect of the TiO_2 particles at high intensities of the UV radiation. The nonlinear dependence of the rate coefficients on the UV intensity was predicted by their model. Thus, the effect of

light intensity on the photocatalytic degradation rate is not straightforward and is dependent on the reactor configuration and the concentration of the TiO_2 photocatalyst.

7.4 Catalyst Loading

The concentration of the photocatalyst is one of the critical parameters that determines the degradation rate of any organic compound. This is dependent on the volume of the solution being treated and the initial concentration of the organic compound. It has been widely observed that the degradation rate increases with an increase in catalyst loading. This is due to the availability of more active catalyst sites at higher concentrations, which results in the generation of more hydroxyl species. However, when loading is increased beyond an optimum value, there is no appreciable increase in the degradation rate. This is because the catalyst particles scatter light, reducing the effective light intensity reaching the bulk reaction solution. In the literature, 0.4–3.5 g L^{-1} of catalyst has been used for the photocatalytic degradation of different organic compounds. Sivalingam et al. [36] observed that the optimum loading of CS TiO_2 for the degradation of dyes is 1 g L^{-1}.

The above argument also holds good when the catalyst particles are immobilized on a substrate like fiberglass, glass slides, glass tubes, etc. In such cases the loading is characterized by the surface coverage of the catalyst, denoted as mass per unit area of the substrate. Hence, the number of coating cycles is a critical parameter, which has to be tuned for the maximum degradation rate. Lim et al. [106] have compared the different dip-coating procedures for the immobilization of TiO_2, 5 coating cycles on woven fiberglass exhibited the highest photocatalytic degradation rate for Methylene Blue. However, in another study, it was found that a direct correlation of optimum catalyst loading for the degradation of organic compounds with the deactivation of microorganisms does not exist. The optimum loading in the case of microorganisms is always lesser than that required for the degradation of organic compounds. For the TiO_2 coated glass sheets, the optimum loading was 0.5 mg cm^{-2} for the deactivation of *E. coli*, while it was 1.1 mg cm^{-2} for the degradation of atrazine and formic acid, under the same conditions of illumination [101]. Therefore, owing to the economics of the catalyst, an optimum concentration is always favorable to study the photocatalytic degradation of organic compounds.

7.5 Presence of Organic Solvents

Organic solvents pose a deleterious effect on the degradation rate of an organic compound. Epling and Lin [107] observed that the degradation rate of Methylene Blue decreased significantly, when 1% of acetonitrile was added to the reaction

mixture. Aarthi and Madras [37] also observed a decrease in the degradation rate of Rhodamine B when the composition of acetonitrile or ethanol was increased in the aqueous medium. This observation is attributed to the fact that the solvation of the CB electrons is reduced in the presence of solvent, which results in the electron–hole recombination. Another possible reason is that the organic solvents scavenge the VB holes, thereby reducing the possibility of generation of hydroxyl radicals. However, organic solvents are beneficial for the partial oxidation of organic compounds to achieve high selectivities for a particular product. This finds applications in the synthesis of fine chemicals by photocatalysis.

7.6 Pollutant Concentration

It is well-known that the rate of degradation is higher at higher concentrations of the organic compound. Especially, for the degradation of colored organic compounds like dyes, the degradation rate exhibits an initial increase with dye concentration, but decreases after a certain critical concentration. This is attributed to the screening of UV radiation by the dye molecules before reaching the catalyst surface. However, the catalyst concentration can be tuned based on the concentration of the organic compound, so that the organic compound can be significantly adsorbed onto the catalyst surface and degraded. Most of the degradation studies have employed a concentration of the organic compounds in the range of 10–200 mg L^{-1}, which agrees well with the concentration of the common pollutants in real wastewater.

7.7 Presence of Anions and Oxidizing Agents

Industrial effluents are composed of a large number of organic compounds, humic substances and inorganic substances, such as anions and metal ions. Hence, an evaluation of the degradability of an organic compound under the influence of such externally added ions is important. It is generally observed that anions like carbonate, bicarbonate, chloride and sulfate ions retard the degradation of organic compounds, in accordance with the following reactions [48–51]:

$$CO_3^{2-} + OH^{\bullet} \longrightarrow CO_3^{\bullet -} + OH^{\bullet -} \tag{37}$$

$$HCO_3^{-} + OH^{\bullet} \longrightarrow CO_3^{\bullet} + H_2O \tag{38}$$

$$Cl^{-} + OH^{\bullet} \longrightarrow Cl^{\bullet} + OH^{-} \tag{39}$$

$$SO_4^{2-} + OH^{\bullet} \longrightarrow SO_4^{\bullet -} + OH^{-} \tag{40}$$

$$SO_4^{\bullet -} + H_2O \longrightarrow SO_4^{2-} + OH^{\bullet} + H^{+} \tag{41}$$

It is clear that all these anions scavenge the hydroxyl radicals to form the respective anion radicals. In the case of the sulfate anion, a sulfate anion radical can result in the formation of hydroxyl radicals according to reaction 41. However, these radicals are again scavenged according to reaction 40, and hence there is a net reduction in the rate of photocatalytic degradation of the organic compound. Azevedo et al. [108] evaluated the effect of saline media on the photocatalytic degradation of phenol and concluded that, at a low concentration of NaCl (2 g L^{-1}), the rate was unaffected, while at a high concentration of NaCl (50 g L^{-1}), there was a drastic reduction in the degradation rate of phenol. However, complete removal and mineralization of phenol was observed. They modeled the reaction using extended-lumped saline kinetics and predicted the time evolution profiles of phenol, intermediates and CO_2. Devi et al. [100] conducted extensive experiments to evaluate the effect of anions on the degradation of anionic and cationic dyes, and found that the presence of sulfate anions result in the highest reduction in the degradation rate of the dyes, while the presence of oxalate anions show the lowest reduction in rate. Thus the reduction in rate due to the presence of different anions for the degradation of Rhodamine B follows the order: ${SO_4}^{2-} > Cl^- > {HCO_3}^- > {NO_3}^- > {CO_3}^{2-} > {C_2O_4}^{2-}$. A similar retardation effect was also observed for the inactivation of microorganisms in presence of TiO_2. According to the results of Rincón and Pulgarin [95], the order of retardation of *E. coli* in presence of different anions is as follows: $Cl^- > {NO_3}^- > {SO_4}^{2-} \gg {HCO_3}^- > {HPO_4}^{2-}$, where the chloride and phosphate ions exhibit the minimum and maximum inhibiting effect, respectively.

The presence of oxidizing agents such as persulfate and H_2O_2 has a positive effect on the degradation rate of the organic compound, which is attributed to the generation of hydroxyl radicals by these oxidizing agents, according to the following reactions [48–51]:

$$S_2O_8^{2-} + e_{CB}^- \longrightarrow SO_4^{2-} + SO_4^{\bullet -} \tag{42}$$

$$H_2O_2 + e_{CB}^- \longrightarrow OH^\bullet + OH^- \tag{43}$$

$$H_2O_2 + O_2^{\bullet -} \longrightarrow OH^\bullet + OH^- + O_2 \tag{44}$$

The sulfate anion radical generated by reaction 42 reacts with water to form a hydroxyl radical by reaction (41). Reactions (43)–(44) are the key reactions for the generation of hydroxyl radicals in presence of H_2O_2. It was previously shown that these two reactions are responsible for the enhanced photocatalytic inactivation of *E. coli* in presence of TiO_2, even at very low concentrations of H_2O_2 (0.3 mM). However, when the concentration of H_2O_2 is higher than the optimum, the following reactions occur, which result in the quenching of the hydroxyl radicals, thereby resulting in a reduction of the degradation rate [48–51]:

$$H_2O_2 + 2h_{VB}^+ \longrightarrow O_2 + 2H^+ \tag{45}$$

$$H_2O_2 + OH^\bullet \longrightarrow H_2O + HOO^\bullet \tag{46}$$

$$HOO^{\bullet} + OH^{\bullet} \longrightarrow H_2O + O_2 \quad (47)$$

Therefore, careful optimization of the concentration of the oxidants is a must for achieving maximum photocatalytic degradation rates.

7.8 Presence of Metal Ions

In the recent past, extensive research has been conducted on the effects of metal ions on the degradation of organic compounds. It is imperative to note that metal ions like Ag^{+}, Hg^{2+}, Cu^{2+}, Pb^{2+}, Cd^{2+}, Ni^{2+} and Cr^{6+} are toxic and have infinite lifetimes. Hence, their accumulation in the environment leads to biomagnification. Reduction of metal ions by photocatalysis is an important subject and many studies have dealt with this aspect [44, 109]. A number of studies have also focused on the simultaneous degradation of organic compounds and reduction of metal ions using TiO_2. Prairie et al. [110] observed that the rate constant for the reduction of Cr^{6+}–Cr^{3+} is strongly dependent on the concentration of salicylic acid, and the rate constant exhibits a sudden drop at salicylic acid concentrations higher than the optimum value. Moreover, the highest degradation rate of salicylic acid was observed in presence of Au^{3+}. An important result of their work shows that only those metal ions whose half-reaction standard reduction potential is greater than 0.3 V (vs NHE) can be treated by photocatalysis.

A careful evaluation of the works of Chen et al. [111], Aarthi and Madras [37], and Kyung et al. [112] shows that the rate of degradation of Rhodamine B decreases in the presence of Cu^{2+}, Fe^{3+}, Zn^{2+} and Al^{3+}, while increasing with the presence of Cr^{6+} and Ag^{+} ions. This suggests that the electronic state of the metal ions also plays a major role in the degradability of the organic compound. Wang et al. [113] studied the photocatalytic degradation of phenol in presence of Cu^{2+} and F^{-} ions using DP-25 TiO_2. The I-order degradation rate coefficient of phenol in presence of different ions exhibited the following trend: $k(Cu^{2+}+F^{-}) > k(F^{-}) > k(Cu^{2+}) > k(\text{without } Cu^{2+} \text{ or } F^{-})$. The observed effect was attributed to the enhanced charge-carrier separation induced by Cu^{2+} and F^{-}.

A common feature in most of the works reporting synergistic degradation of organic compounds in the presence of metal ions is that the pH of the reaction mixture was in the acidic regime. For example, the reduction of Cr^{6+}–Cr^{3+} occurs in the presence of protons according to the following reaction [114]:

$$2Cr_2O_7^{2-} + 16H^{+} \rightarrow 4Cr^{3+} + 8H_2O + 3O_2 \quad (48)$$

Hence, an acidic medium can provide excess protons for the reduction of Cr^{6+} compared to a neutral or basic medium. Moreover, metal ions like Cr^{6+} and Cu^{2+} precipitate as hydroxides in the basic pH regime, which prevents them from getting adsorbed onto the TiO_2 surface. In a recent study, Vinu and Madras [114] observed that the presence of phenol accelerated the reduction of Cu^{2+}–Cu^{+}, while this was not possible in the absence of phenol (Fig. 8). The presence of Cu^{2+} ions

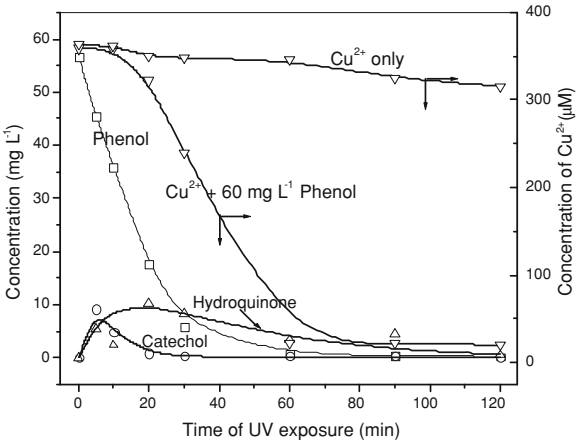

Fig. 8 Concentration profiles of phenol and Cu^{2+} during the simultaneous oxidation–reduction of phenol+Cu^{2+} using CS TiO_2. The phenolic intermediates, viz., catechol and hydroquinone were observed only in the presence of Cu^{2+} [114]

did not significantly alter the degradation rate of phenol, while the presence of Cr^{6+} enhanced the degradation of phenol.

Sun et al. [115] showed that, among the different metal ions like Cu^{2+}, Fe^{3+}, Mn^{4+}, Ce^{4+}, V^{5+} and Cr^{6+}, only Cr^{6+} accelerated the photooxidation of 4-chlorophenol in presence of visible light. Therefore, it can be summarized that the simultaneous degradation-reduction of such two-component systems containing an organic compound and a metal ion is dependent on the pH of the solution, concentration of the metal ions and the organic compound, adsorption of the metal ion and the electronic states of the metal ions.

8 Mechanistic Models for Photocatalytic Degradation

8.1 Models for the Degradation of Organic Compounds

It is well reported that the rate of photocatalytic degradation of the organic compounds follows the classical Langmuir–Hinshelwood (L–H) kinetics [116]. Sivalingam et al. [36] derived the rate equation for the photocatalytic degradation of dyes by incorporating the reactions including charge-carrier generation, recombination, adsorption–desorption of the substrate, generation of hydroxyl radicals and the oxidation of the adsorbed organic compound by hydroxyl radicals and holes. The rate equation, which resembles the L–H equation, is given by:

$$-r_A = \frac{K_0((k_{0h}/K_0) + k_0)C_A}{1 + K_0 C_A} \tag{49}$$

where, r_A denotes the rate of consumption of the organic compound, C_A is the concentration of the organic compound, and K_0 is the equilibrium adsorption rate coefficient, which includes the adsorption of the organic compounds and hydroxyl radicals. The rate coefficients k_{0h} and k_0 signify the oxidation of the organic

compound by direct hole attack and by the hydroxyl radicals, respectively. Hence, the compound rate coefficient $k_r = (k_{0h}/K_0) + k_0$ denotes the oxidation of the organic compound. A simple way to determine the rate coefficients K_0 and k_r is the initial rate method. In this method, the equation is inverted and rearranged so that a plot of $1/C_{A0}$ versus $1/r_{A0}$ yields the slope and intercept, from which K_0 (in L mg^{-1}) and k_r (in mg L^{-1} min^{-1}) can be evaluated. The equation is given by

$$-\frac{1}{r_{A0}} = \frac{1}{k_r K_0}\frac{1}{C_{A0}} + \frac{1}{k_r} \tag{50}$$

It is worthwhile to note that the equilibrium adsorption coefficient, K_0 determined from the L–H equation is different from the adsorption coefficient that is determined by the Langmuir adsorption isotherm. This is because the equilibrium adsorption coefficient determined by the Langmuir isotherm denotes the adsorption–desorption of the organic compound in the dark, while K_0 signifies the adsorption of the organic compounds onto the catalyst surface and the desorption of the products from the surface during the photoreaction. Hence, it is imperative to note that K_0 is dependent on other reaction parameters including the intensity of UV irradiation, concentration of oxygen and the catalyst concentration.

As most of the organic compounds are present at trace levels in the atmosphere or effluent stream, the term $K_0 C_A \ll 1$ in the denominator of Eq. 49. Hence, the rate equation can be simplified to a first-order equation with 'k' as the first-order rate constant signifying the degradation of the organic compound [39].

$$-r_A = -\frac{dC_A}{dt} = kC_A \tag{51}$$

The solution of the above equation is given by $C_A = C_{A0}\exp(-kt)$. The rate coefficient, k, can be determined by a linear plot of $\ln(C_{A0}/C_A)$ versus t. The value of the rate coefficient reported in the literature for the degradation of organic compounds varies over a wide range and, therefore, it is difficult to establish a specific range of variability. This is because the rate coefficient is dependent upon the type of the catalyst (anatase/rutile TiO_2), intensity of the UV radiation, catalyst loading and other reaction parameters like pH, and the presence of anions and cations.

Li et al. [117] developed a kinetic model for the rate of degradation of Rhodamine B dye in presence of a TiO_2-coated, activated carbon catalyst by including the fractional surface coverage of the hydroxyl radicals and the dye, on the catalyst surface. The L–H parameters were found to depend on the intensity (I) of the UV radiation according to the following equations:

$$k_r^{-1} = \alpha I^{-1/2} + \beta \tag{52}$$

$$K_0 = \eta I^{-1/2} + \varpi \tag{53}$$

where, α, β, η and ω are lumped constants, expressed in terms of the rate coefficients and signifying the individual steps. They have observed good agreement of the model with the experimental data at different light intensities.

Wu and Chern [105] adopted a cyclic network reduction technique to derive the rate expression for the degradation of Methylene Blue. The rate of decomposition of Methylene Blue was found to depend on the initial concentration of the dye, light intensity, TiO_2 loading and dissolved oxygen concentration. The rate expression is given by:

$$-r_A = \frac{k_a' C_A}{1 + k_b' C_A} \tag{54}$$

where, $k_a' = \frac{k_4[h\nu][TiO_2]}{1+k_1[h\nu]}$ and $k_b' = \frac{k_2+k_3[h\nu]}{1+k_1[h\nu]}$. The concentration profiles were simulated by integrating Eq. 54 in the limits $C_A|_{t=0} = C_{A0}$ and $C_A|_{t=t'} = C_{At}$. The rate coefficients were determined by nonlinear curve fitting of the following expression with the experimental data:

$$\ln\left(\frac{C_{At}}{C_{A0}}\right) + k_b'(C_{At} - C_{A0}) = -k_a' t \tag{55}$$

Almquist and Biswas [118] investigated the effect of dissolved oxygen on the kinetics of degradation of phenol in presence of DP-25. Their results show that dissolved oxygen has an inhibiting effect on the degradation of phenol when the concentration of phenol is of the order of the solubility of oxygen in water. They developed a three-parameter model that describes the dependence of the degradation rate on the concentration of phenol and dissolved oxygen. The rate equation is given by:

$$-\frac{dC_A}{dt} = \frac{bC_{O_2}C_A\left\{\sqrt{1 + a/C_{O_2}} - 1\right\}}{1 + cC_A} \tag{56}$$

The model parameter 'a' depends on the light intensity profile inside the reaction slurry, light absorption and the efficiency of electron-hole formation and recombination. The parameters 'b' and 'c' depend mainly on the type of TiO_2. The parameters were determined by nonlinear curve fitting. Therefore, the differing kinetic equations suggest that, although L–H and the first-order model satisfactorily describes the overall kinetics of degradation of organic compounds, more thorough models must be used to unravel the effects of different reaction parameters like the UV light intensity, catalyst loading, oxygen concentration and the mode of reactor operation.

8.2 Modeling of Microbial Inactivation

The kinetics of photocatalytic disinfection of microorganisms is quite different from that of the organics because the inactivation profiles are characterized by three distinct regimes. In the first regime, a "shoulder" or a slow deactivation of the microorganisms occurs due to the self-defense and auto-repair mechanisms of the bacterial

cell membrane against the hydroxyl radicals [119]. Once the hydroxyl radical concentration builds up in the system and a certain number of critical molecules are denatured, perforation of the bacterial membrane occurs, as the anti-stress enzymes are unable to prevent the membrane from oxidation. Thus, in the second regime, a log-linear reduction in concentration of the microorganism is observed. The last part of the deactivation process is characterized by a slow reduction in concentration or tailing of the concentration profile, due to the release of organic compounds into the medium, which competes with the inactivation of the microorganism.

Several empirical models have been proposed to account for the different regimes of deactivation of microorganisms [120]. These include a delayed Chick-Watson, modified Chick-Watson, Hom and modified Hom equations. The modified Hom equation, which fits well with the bacterial concentration profile has three adjustable parameters and is expressed as:

$$\log \frac{C_0}{C} = k_1[1 - \exp(-k_2 t)]^{k_3} \tag{57}$$

where, C_0 and C are the initial concentration and concentration at time 't' of the microorganism in the system. The parameters k_1, k_2 and k_3 in the above model have no physical significance. Therefore, rigorous mechanistic models are necessary to describe the kinetics of the deactivation of microorganisms. Initially, the mechanism of rupturing the cell wall of the microorganism, thereby inactivating the organism, was represented as a series of consecutive events of different damage levels [120, 121]:

$$C_0 \xrightarrow{k_1} C_1 \xrightarrow{k_2} C_2 \xrightarrow{k_3} C_3 \cdots \xrightarrow{k_n} C_n \tag{58}$$

where, k_i denotes the kinetic rate coefficient for the damage from level $i - 1$ to i. Labas et al. [121] coupled the radiation transport equation with this model and observed that the threshold limit for bacterial damage corresponds to two levels ($n = 2$). Other parameters in their model correspond to the inactivation rate coefficient k, and the reaction order with respect to the local volumetric rate of photonic absorption of the bacteria.

Marugán et al. [120] recently proposed a modified mechanism for the deactivation of *E. coli*, represented as:

$$C_\mathrm{undamaged} \xrightarrow{k_1} C_\mathrm{damaged} \xrightarrow{k_2} C_\mathrm{inactivated} \xrightarrow{k_3} C_\mathrm{product} \tag{59}$$

where, $C_\mathrm{undamaged}$ denotes the undamaged population of the microorganism, C_damaged denotes the lumped population at all intermediate levels of damage, $C_\mathrm{inactivated}$ denotes the microorganisms in the inactive state and C_product denotes the products of microbial cell lysis, which are released into the reaction medium. The L–H-like model for the above mechanism is given by:

$$\frac{\mathrm{d}C_\mathrm{undamaged}}{\mathrm{d}t} = -k \frac{KC^\mathrm{n}_\mathrm{undamaged}}{1 + KC^\mathrm{n}_\mathrm{undamaged} + KC^\mathrm{n}_\mathrm{damaged}} \tag{60}$$

$$\frac{dC_{damaged}}{dt} = k\frac{KC^{n}_{undamaged} - KC^{n}_{damaged}}{1 + KC^{n}_{undamaged} + KC^{n}_{damaged}} \quad (61)$$

where, the rate coefficients k, K and n correspond to the interaction of the hydroxyl species with the microorganism, microorganism with TiO_2, and the products of bacterial lysis with the hydroxyl species, respectively. The above expression is based on the assumption that the rate coefficients for the intrinsic reaction steps for the undamaged and the damaged cells are the same. Thus, the rate coefficients K, k and n signifying the pseudo-adsorption, inactivation and inhibition, represent the initial lag, log-linear decrease and final lag phases of the bacterial disinfection profiles, respectively. This model has been validated for the deactivation of *E. coli* with different catalysts of varying concentrations, and in presence of anions like chloride, bicarbonate and phosphate, and humic acids [122].

8.3 Modeling of Multicomponent Systems

Industrial effluents are composed of a mixture of different organic compounds (dyes, phenolics, chlorinated compounds) and metal ions. The rate of degradation of an organic compound in the presence of another will be different from individual degradation rates. Therefore, kinetic modeling of multicomponent systems yields useful information on the interaction between the different species in the system, competition of the reactants and products for the active sites, and the mechanism of degradation. Priya and Madras [123] studied the photocatalytic degradation of mixtures of 4-chlorophenol and 4-nitrophenol to simulate the industrial effluent. They modeled the rate of degradation of chlorophenol (cp) and nitrophenol (np) using the following rate equations with individual L–H rate parameters (k_{cc}, K_{cp}, k_{nn} and K_{nn}) and interaction parameters (k_{cn} and k_{nc}):

$$-r_{cp} = \frac{(k_{cc} - k_{cn}C_{np})C_{cp}}{1 + K_{cp}C_{cp} + K_{np}C_{np}}; \quad -r_{np} = \frac{(k_{nn} - k_{nc}C_{cp})C_{np}}{1 + K_{cp}C_{cp} + K_{np}C_{np}} \quad (62)$$

The above model accounts for the competitive inhibition of the rate of degradation of cp by np, and vice-versa. The denominator in the above equations accounts for the competition of cp and np for the active site of TiO_2. By linearizing the above expressions, the rate coefficients were determined. Based on the values of k_{cn} and k_{nc}, it was found that the degradation of chlorophenol was unaffected by the presence of nitrophenol, while the degradation of the nitrophenol was significantly affected by the presence of the chlorophenol.

Similarly, when a metal ion is present in the system along with an organic compound, simultaneous oxidation and reduction reactions occur, and the kinetics of the reaction is affected by the complex interaction of the organic compound and metal ion with the TiO_2 surface. A detailed discussion on this topic is available in Sect. 7.8. The retardation of the rate of degradation of dyes in presence of metal

ions was modeled by Aarthi et al. [37], and their kinetic model relates the rate of degradation of the dye (r_D) with the concentration of the dye [D] and the metal ion [M^{n+}]. The equation is given by:

$$-\frac{1}{r_D} = \left(\frac{1}{[D]} + K_2\right)\frac{(1 + K_6[M^{n+}])}{(k_0 + K_6 k_7[M^{n+}])} \tag{63}$$

The lumped rate coefficients in the above model, viz. K_2, K_6, k_0 and k_7, were determined by nonlinear regression, and the model was validated for the degradation of different dyes, including Rhodamine B [37], Rhodamine 6G [37], Sulforhodamine B [37] and Azure B [124], in presence of Cu^{2+}. One shortcoming of this model is that it does not account for the concomitant reduction of metal ions during the degradation of the organic compound. With this in mind, Vinu and Madras [114] modeled the simultaneous and synergistic degradation of phenolic compounds (phenol and 4-nitrophenol), and the reduction of metal ions (Cu^{2+} and Cr^{6+}), by assuming competitive adsorption of metal ions and the phenolic compounds onto the TiO_2 surface. The steady-state rates through the individual phenol degradation and metal ion reduction pathways, derived using the network reduction technique, are given by:

$$\left(-\frac{1}{r_{Ph,0}} - K_2\right) = \frac{1}{[Ph]_0}\left(\frac{1}{K_1} + \frac{[M^{n+}]}{K_3}\right) \tag{64}$$

$$\left(-\frac{1}{r_{M^{n+},0}} - K_5\right) = \frac{1}{[M^{n+}]_0}\left(\frac{1}{K_4} + \frac{[Ph]}{K_6}\right) \tag{65}$$

where, $r_{Ph,0}$ and $r_{Mn+,0}$ denote the initial rate of degradation of phenolic compound and the reduction of metal ions, respectively. This model accounts for the contribution of the metal ions for the rate of degradation of the phenolic compound and vice versa. The lumped rate coefficients K_2 and K_5 were determined by individually degrading phenolic compounds and metal ions, and the other rate coefficients were evaluated by conducting multiple experiments at different phenol and metal ion concentrations. Using this model, the rate coefficients can be determined uniquely by a simple linear regression.

8.4 Modeling of Degradation Intermediates

The intermediates formed during the degradation of organic compounds can have a deleterious effect on the overall degradation rate, since these compounds compete for the active sites of the catalyst. Hence, by knowing the formation and consumption rate of the different intermediates, the relative importance of each of them on the overall mineralization of the parent compound can be assessed. Previous studies on the degradation of phenolic compounds, dyes and pesticides have monitored the concentration of the various intermediates during degradation.

For example, the predominant intermediates observed during the degradation of phenol include catechol, hydroquinone, hydroxy hydroquionone, benzoquinone and oxalic acid. The kinetics of formation and consumption of these intermediates was modeled by considering a simple series reaction mechanism with first-order reactions [39, 40], represented as:

$$\mathrm{A} \xrightarrow{k_f} \text{Intermediate} \xrightarrow{k_c} \text{Product} \tag{66}$$

where, k_f and k_c are the formation and consumption rate coefficients of the intermediates. By writing rate equations for A, intermediate and the product, an expression for the concentration of the intermediate can be derived as [125]:

$$\frac{C_{int}}{C_{A0}} = \frac{k_f}{k_c - k_f}(\exp(-k_f t) - \exp(-k_c t)) \tag{67}$$

The concentration profiles of the primary hydroxylated species show an initial increase and subsequent decrease with time due to the formation of secondary hydroxylated species. Hence, there is a time (t_{max}) at which the concentration of the intermediate is maximum (C_{max}). Therefore, by differentiating the above equation with respect to t and C_{int}, expressions for t_{max} and $C_{int,max}$ were derived as [125]:

$$t_{max} = \frac{\ln(k_f/k_c)}{k_c(k_f/k_c - 1)} \tag{68}$$

$$\frac{C_{int,max}}{C_{A0}} = \left(\frac{k_f}{k_c}\right)^{1/(1-k_f/k_c)} \tag{69}$$

Thus, by solving these two equations with t_{max} and $C_{int,max}$ from the experimental data, k_c and k_f can be determined. More importantly, the ratio k_c/k_f, which signifies the relative rate at which the intermediate is consumed, can be used as a quantifying factor to assess the stability of the different intermediates and the effective mineralization of the parent compound. The formation of catechol and hydroquinone during the photocatalytic degradation of phenol in presence of Cu^{2+} ions and CS TiO_2 is depicted in Fig. 8. The curves for catechol and hydroquinone represent the model fits.

9 Visible Light Degradation of Organic Compounds

9.1 Second Generation TiO_2 Photocatalysts

The first generation TiO_2 or pristine TiO_2 proves to be an efficient photocatalyst in the UV region. However, the wide band-gap (3.2 eV) of anatase TiO_2, corresponding to an absorption threshold of 390 nm, limits its use in the visible range

Table 6 Effect of different metal ion substitutions in TiO_2 for the photocatalytic degradation of organic compounds

Sl. No.	Organic compound	Substituted metal ion in TiO_2	Results	Reference
1	CCl_4 and $CHCl_3$	Fe^{3+}, Mo^{5+}, Ru^{3+}, Os^{3+}, Re^{5+}, V^{4+}, Rh^{3+}, Co^{3+}, Al^{3+}	Co^{3+} and Al^{3+} doping reduces the photoactivity, while all other metal ions in the concentration range from 0.1 to 0.5 at. % enhance the photoactivity	[126]
2	Oxalic acid	Cr^{3+}, Fe^{3+}, V^{5+}	The photoactivity of all the samples was lower compared to bare TiO_2	[127]
3	2-Chlorophenol	Nd^{3+}, Pd^{2+}, Pt^{4+}, Fe^{3+}	Order of photoactivity: $Nd^{3+} > Pd^{2+} > Pt^{4+} \approx$ undoped $> Fe^{3+}$	[128]
4	5,5-Dimethyl-1-pyrroline N-oxide (DMPO spin trap)	Cr^{3+}, Mn^{2+}, Co^{2+}	All the metal ion-doped samples exhibit a lower photocatalytic activity for the generation of DMPO-OH and DMPO-O_2^- compared to undoped DP-25	[129]
5	4-Nitrophenol	Cu^{2+}, Fe^{3+}, Ce^{4+}, Zr^{4+}, V^{5+}, W^{6+}	Order of photoactivity: undoped CS $TiO_2 > Fe/TiO_2 > W/TiO_2 > Ce/TiO_2 > Zr/TiO_2 > V/TiO_2 \approx Cu/TiO_2$	[130]
6	Orange II	La^{3+}, Ce^{4+}, Pr^{3+}, Nd^{3+}, Sm^{3+}, Eu^{3+}, Dy^{3+}, Gd^{3+}	High visible light photoactivity compared to undoped TiO_2 in the concentration range of 0.5–1 wt%	[131]

(400–800 nm) in practical applications. Moreover, solar radiation is comprised of c.a. 50% visible radiation and less than 5% UV radiation. Hence, extending the spectral absorption of TiO_2 to the visible region is vital for the development of energy efficient degradation processes.

Second generation TiO_2 catalysts encompass a wide variety of the cationic and anionic substituents in TiO_2. The cationic substituents mainly include metal ions, while the anionic substituents include C, N and S. Numerous studies have examined the substitution of lower valent (+1, +2, +3), iso valent (+4) and higher valent (+5, +6) metal ions in the lattice of TiO_2 for the photocatalytic degradation of organic compounds. This includes noble metals, transition metals, lanthanide metals and alkaline metals. Table 6 [126–131] presents a list of the various studies conducted on the photocatalytic activity of metal ion-doped TiO_2. Although there is a general consensus that metal ion doping extends the absorption spectrum of TiO_2 to the visible region, the photocatalytic activity of the metal ion-doped TiO_2 compared to the undoped TiO_2 varies across different studies. From the table, it is evident that doping of some metal ions enhances the photoactivity, while others result in a reduction of photoactivity.

Choi et al. [126], by studying the transient absorption decay of the trapped electrons, showed that the dopant energy levels serve as trap sites for the electrons and holes, apart from the surface trap sites. The low activity exhibited by metal

ion-doped TiO_2 is due to these states acting as recombination centers. Hence, the photoactivity of metal ion-doped TiO_2 strongly depends on the dopant concentration, energy level of the dopant within the TiO_2 lattice, *d*-electronic configuration, distribution of dopant, interfacial charge transfer and light intensity. Nagaveni et al. [130] conducted a thorough photoluminescence study of the different metal ion-doped TiO_2 ($M_xTi_{1-x}O_{2\pm\delta}$), synthesized by the solution combustion technique, and observed a reduction in the emission intensity of the metal ion-doped samples. The metal ions form inter-band energy levels above the valence band or below the conduction band, which result in lower band gap of the doped TiO_2 materials. Serpone et al. [127] showed that doping of Cr^{3+}, Fe^{3+} and V^{5+} in the lattice of TiO_2 results in a lower photoactivity for the oxidation of oxalic acid, but an enhanced activity for the photoreduction of water to H_2. Similarly, Pd^{2+} ion substitution in CS TiO_2 was found to be beneficial for gas phase CO oxidation, NO reduction and NO decomposition [132], while it exhibited a negative effect for liquid phase degradation of organic compounds [133]. This shows that a generalization of the activity of metal doped TiO_2 compared to the undoped TiO_2 is not possible for a wide class of reactions.

Another method by which metal ions can be incorporated in TiO_2 is by impregnation on the surface. Paola et al. [134] investigated the effect of different transition metals impregnated TiO_2 for the photocatalytic degradation of aliphatic and aromatic compounds and found that the highest mineralization efficiency was obtained with bare TiO_2. In addition to the above result, Vinu and Madras [133, 135] showed that TiO_2 impregnated with Pd or Ag exhibits higher photoactivity compared to doped-TiO_2. The higher activity exhibited by the metal ion-impregnated TiO_2 is attributed to the formation of a Schottky barrier, which results in the scavenging of electrons and holes, thereby preventing unfavorable recombination reaction.

While metal ions are substituted for the Ti atoms in the lattice, anions are substituted for oxygen in the oxide. Hence, these are represented as $TiO_{2-x}D_x$, where D is usually N, C or S. The first study on anion-substituted TiO_2, $TiO_{2-x}N_x$, was carried out by Asahi et al. [136] for the photocatalytic degradation of Methylene Blue and gaseous acetaldehyde in presence of visible radiation. Based on X-ray photoelectron spectroscopic analysis, they observed an optimum concentration of N to be 0.25 atomic%. Khan et al. [137] incorporated C in TiO_2 by flame pyrolysis, which shows a band gap of 2.32 eV, and high activity for photosplitting of water (photoconversion efficiency = 8.35%). Unlike the cation-doped TiO_2, anion-doped TiO_2 exhibits a high photoactivity in the visible region compared to undoped and commercial DP-25 due to narrowing of the band-gap. In fact, the band gap narrowing of N doped TiO_2 was attributed to the mixing of N 2p and O 2p energy levels. This requires the elevation of valence band maximum or the lowering of conduction band minimum by the introduction of new energy level of the anion dopant, with a more homogeneous distribution and without a loss of the crystal structure of the host TiO_2. The rules for any non-metal to be substituted for oxygen in TiO_2 to elevate the valence band, are as follows [138]: (i) the electronegativity of the non-metal dopant should be lesser than that of oxygen, and

(ii) the radius of the dopant should be comparable to that of oxygen for a more uniform distribution.

Serpone [139] demonstrated that the visible light activity of the anion-doped TiO_2 is not due to the narrowing of the band-gap, but due to the defects associated with the oxide ion vacancy, which results in the formation of color centers. Color centers are essentially a single or a pair of electrons associated with an oxygen vacancy. For MgO, it has been shown that the ground state of the color centers lie above the O 2p valence band. Table 7 [140–144] shows the different studies on the anion-doped TiO_2 for the visible light degradation of organic compounds.

9.2 *Heterostructuring of TiO_2*

Heterostructuring refers to the modification of the surface of pristine TiO_2 by employing (i) narrow band-gap semiconductor dopants (like CdS, PbS, CdSe, Bi_2S_3), (ii) dyes as sensitizers and (iii) co-catalysts [138]. Different schemes of charge-carrier transfer have been proposed for heterostructured TiO_2 materials, viz. traditional charge-carrier transfer, sensitization, indirect Z-scheme, direct Z-scheme, vectorial electron transfer and co-catalyst coupling. The main idea of these heterostructuring procedures is to isolate the electrons and holes at two different reaction sites in order to prevent recombination. This enhances the efficiency of simultaneous oxidation and reduction reactions. Moreover, the incorporation of small band-gap semiconductors, dyes and co-catalysts, increases the probability of absorption in the visible range. Liu et al. [138] reviewed such schemes in terms of their mechanisms, materials and the key issues involved in their implementation. Figure 9 depicts the two different modes of charge transfer in presence of a sensitizing dye and a narrow band-gap semiconductor. Some important design considerations for the heterostructured systems, for effective interfacial charge transfer, are as follows:

- The main semiconductor (TiO_2) and the dopant semiconductor need to have suitable electronic structure, i.e., the dopant should have a higher conduction band minimum and valence band maximum compared to TiO_2, for the smooth injection of electrons downhill from the conduction band of the dopant, and the transfer of holes uphill to the valence band of the dopant.
- The above condition is also applicable for sensitizers, although there is no transfer of holes to the HOMO. Moreover, high surface area of TiO_2 is necessary for the enhanced adsorption of the sensitizer.
- Intimate contact between the two different phases (e.g., a p–n junction in the case of traditional transfer or Ohm/Schottky contact in the case of co-catalysts) is necessary.

Table 8 [145–154] presents the different studies on the sensitized degradation of organic compounds using modified TiO_2 materials. It is clear that a wide variety of sensitizers like narrow band-gap semiconductors, organic dyes and conjugated polymers are being coupled to TiO_2 to enhance the visible light response.

Table 7 A survey of the recent studies on the photocatalytic degradation of organic compounds using anion-doped TiO_2

Sl. No.	Organic compound	Photocatalyst/loading	Light source	Initial concentration	% degradation	Time taken	Reference
1	Orange G, RBBR, Methylene Blue	CS TiO_2; 1 g L^{-1}	Sunlight; 753 W m^{-2}	25, 100, 100 ppm	100, 80, 90	2, 1.5, 4 h	[140]
2	Methylene Blue	C-doped TiO_2; 1 g L^{-1}	Sunlight; 21.28 W m^{-2}	10 ppm	100	1 h	[141]
3	2,4-Dichlorophenol, Acid Orange 7	C deposited TiO_2; 1 g L^{-1}	1,000 W HL	50, 20 ppm	60, 100	5, 4 h	[142]
4	Reactive Brilliant Red X-3B	C, N, S—tridoped mesoporous TiO_2; 1.5 g L^{-1}	250 W HL	100 ppm	70	2 h	[143]
5	Methylene Blue	$Ti_{1-x}Ce_xO_{1-y}N_y$; x = 0.007; 1 g L^{-1}	30 W FL	15 ppm	100	4 h	[144]

RBBR—Remazol brilliant Blue R; HL—halogen lamp; FL—fluorescent lamp

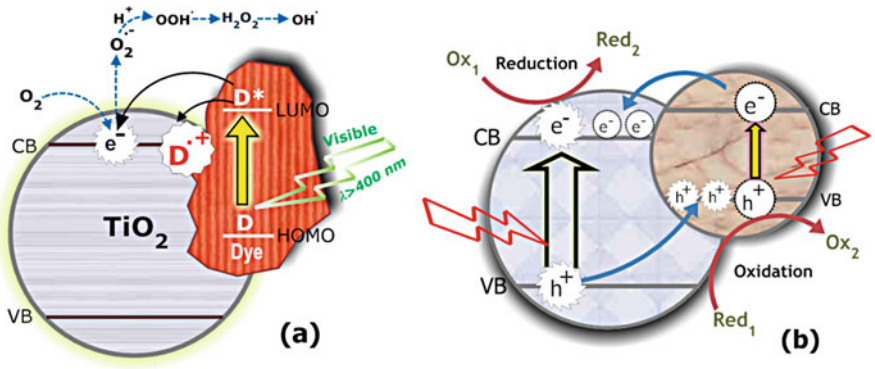

Fig. 9 Mechanism of charge carrier transfer in **a** dye sensitized TiO_2, and **b** narrow band gap semiconductor coupled TiO_2

Moreover, the time taken for the complete degradation of the organic compounds varies from 1 to 10 h, which shows the importance of optimizing the various reaction conditions like the initial concentration of the organic compound, catalyst loading and the intensity of the light source. Hence, a fair comparison of the photoactivity of the different modified TiO_2 materials requires the evaluation of the kinetic rate coefficients of degradation.

10 Photocatalysis in Practice

10.1 Immobilization of TiO_2

The photocatalytic degradation reactions considered thus far have been conducted in small volume (0.1–10 L) batch reactors, usually in immersion well photoreactors [36], in which the catalyst particles are suspended and continuously stirred in the reaction mixture. While this configuration is beneficial for the high mass transfer of the reactants and products on the catalyst surface, which results in high degradation rates of organic compounds, this mode of operation is not suitable for large-scale applications involving large volumes of effluents, due to the inherent problem associated with the separation of the catalyst particles after the completion of the reaction. This escalates the costs related to the operation of the unit due to the complex downstream operations involved.

A solution to the above scale up issue is to immobilize the catalyst on a suitable support material. Many different supports have been explored for the immobilization of TiO_2, viz. glass beads [155], flexible fiber glass cloth [156], glass tubes [157], cotton [158], stainless steel [159], ZnO tetrapods [160], silicone rubber film [161], PTFE mesh sheets [162], polystyrene beads [163], low density support (perlite) [164] and porous lavas (pumice stone) [165]. A good support is

Table 8 Survey of the recent studies on sensitized degradation of organic compounds using modified TiO_2

Sl. No.	Organic compound	Sensitizer in TiO_2	Light source	Initial concentration	% degradation	Time taken	Reference
1	Methyl Orange, 4-Chlorophenol	MoS_2 and WS_2	300 W WHL	20 μM		30–120 min	[145]
2	Methyl Orange	Poly(3-hexyl thiophene)	300 W IWL	10 ppm	90	10 h	[146]
3	4-Chlorophenol	Al tetracarboxy phthalocyanine	500 W HL	0.23 mM	90	8 h	[147]
4	2,3-Dichlorophenol	Poly(thiophene)	150 W HPSL	20 ppm	50	7 h	[148]
5	2,4-Dichlorophenol	Xanthene dyes	500 W HL	16.3 mg L^{-1}		5 h	[149]
6	Phenol	Metallo phthalo-cyanines	100 W HL	100 ppm	90	1 h	[150]
7	Terbutyl azine	Rose Bengal (10 ppm)	500 W XL	5 ppm	50	2 h	[151]
8	Atrazine	Tetra(4-carboxy phenyl) porphyrin	XL	20 ppm	80	1 h	[152]
9	Trichloroacetate and CCl_4	$Pt/TiO_2/Ru^{II}L_3$ (10 μM)	450 W XL	1 mM		2–3 h	[153]
10	Methylene Blue and 4-Chlorophenol	CdS quantum dot	300 W WHL	100 ppm, 100 μM	95, 70	3, 4 h	[154]

WHL—Tungsten halogen lamp; IWL—iodine tungsten lamp; HL—halogen lamp; XL—xenon arc lamp; HPSL—high pressure sodium lamp

characterized by its inertness to UV radiation, non-toxic nature, corrosion and erosion resistance at highly acidic and basic conditions and good adhesion to the catalyst particles. The different immobilization procedures include dip-coating, pasting, spray coating from suspension, sol–gel technique, CVD, sputtering and electrophoretic deposition. Usually, catalyst particles are coated many times on the supports to achieve better photocatalytic activity. However, excessive layers results in the detachment of the outer catalyst layers and cracking of the surface. Lim et al. [106] compared four different dip-coating methods for the mineralization of Methylene Blue and concluded that a hybrid method with 5 coating cycles and a calcination period of 1 h at 500°C yielded the best results. Moreover, the suitability of the substrates for immobilization followed the order: woven fiberglass $\approx$ fiberglass $\gg$ Al plate $\geq$ glass plate. However, the optimum number of coating cycles for the effective degradation of an organic compound is different from that required for the degradation of a microorganism. This was demonstrated in wall and fixed-bed reactors, where 2 dip-coating cycles exhibited the highest deactivation of *E. coli*, whereas, 3 dip-coating cycles were necessary for the effective degradation of Methylene Blue [166].

The degradation of organic compounds and microorganisms is, however, always lesser in an immobilized catalyst system compared to the suspended catalyst system. This is because of the reduction in the surface area of the catalyst, which results in the lesser adsorption of the reactants. Moreover, there is a significant reduction in activity of the immobilized catalyst with time due to the eventual loss of the catalyst particles from the surface, and the fouling of the catalyst, caused by the adsorption of the degradation products on the catalyst surface. Although the adsorbed products can be eliminated by calcination of the immobilized catalyst, this might affect the surface characteristics of the catalyst. Rao et al. [167] evaluated the reduction in activity of TiO_2 on different supports for the degradation of Acid Orange 7 and observed that the reductions in efficiency were a factor of four on TiO_2/polymer film, five on TiO_2/cellulosic fibers and ten on TiO_2/pumice stone after a period of 4 weeks. In a different study, Nakashima et al. [162] investigated the degradation of endocrine disrupting compounds like 17β-estradiol, bisphenol-A and 2,4-dichlorophenol using TiO_2 immobilized on PTFE mesh sheets. They observed 4.5 times enhancement in the mass transfer rate of these compounds when the PTFE sheets were rotated at 60 rpm compared to conventional circulation of the reaction mixture. In spite of the shortcomings, the recent research in the development of novel supports and immobilization protocols makes immobilized systems the preferred configuration for large-scale utilization of photocatalysis for the degradation of water pollutants.

10.2 Photocatalytic Reactor Modeling

Small scale batch reactors are widely used for the evaluation of the catalytic activity of novel photocatalytic materials, and for establishing the mechanism and kinetics of photocatalytic degradation reactions. Nevertheless, industrial decontamination

of effluents requires large volumes to be processed. Hence, continuous operation is the preferred method, with catalyst particles immobilized on suitable supports. Different reactor configurations have been found suitable for photocatalytic degradation reactions, which include, thin film, flat plate, fluidized bed, packed bed, rotating disc, fountain type slurry, tubular, membrane, fiber, monolithic, bubble column, air-lift loop, Taylor-vortex flow and concentrating and non-concentrating solar reactors. A detailed description of the various photocatalytic reactor configurations is available elsewhere [168]. Given a wide range of reactor configurations, it is important to critically evaluate them based on the mass transfer limitations, spectral energy distribution of the light source, axial and radial dispersion of the reactants, catalyst layer thickness and energy efficiency, in order to find the best configuration for a particular class of pollutant and reaction conditions. Therefore, in depth modeling of these reactors based on the first principles chemical engineering approach is important.

The key component that distinguishes photocatalytic reactors from conventional reactors is the dependence of the kinetics of the reaction on the irradiance of the light source. Hence, models for photocatalytic reactors incorporate local volumetric rate of energy absorption (LVREA) in the rate expression. This is represented as [169–171]:

$$r = k_{\mathrm{R}}\left[e_{\lambda}^{\mathrm{a},v}(\underline{x})\right]^{n}\frac{K_{\mathrm{R}}C_{\mathrm{R}}}{1+K_{\mathrm{R}}C_{\mathrm{R}}} \tag{70}$$

where, r denotes the rate of the reaction per unit reactor volume, k_{R} denotes the rate coefficient for the degradation of the pollutant R, which is independent of light intensity, K_{R} denotes the equilibrium adsorption coefficient, C_{R} denotes the concentration of the pollutant, and $e_{\lambda}^{\mathrm{a},v}$ signifies the LVREA, which is dependent on the position vector $\underline{x}$ in the reaction space, and the exponent n signifies the dependence of the rate on LVREA. The selection of n is based on the light intensity and was discussed in Sect. 7.3. An expression for LVREA is [171]:

$$e_{\lambda}^{\mathrm{a},v}(\underline{x}) = \kappa_{\lambda}(\underline{x})G_{\lambda}(\underline{x}) \tag{71}$$

where, κ_{λ} is the spectral volumetric absorption coefficient, which is a function of the concentration of the absorbing species, and G_{λ} is the spectral local incident radiation [171].

Equation 70 shows that the rate follows L–H kinetics, but any appropriate rate form (like first-order or multicomponent L–H) can be used, based on the influence of the different reactants. Thus, by incorporating the rate of the reaction in the mass balance or continuity equations, and solving the equation with appropriate boundary conditions at steady-state, yields the concentration profiles of the reactant as a function of space inside the reactor. Similarly, by solving the momentum balance equation, the velocity profiles can be obtained. Jarandehei and Visscher [172] carried out a computational fluid dynamics simulation of a flat plate photocatalytic reactor with a serpentine geometry for the photocatalytic degradation of

trichloroethylene. They found that the kinetics of the reaction is better captured by the L–H model than the first-order model. By analyzing the velocity and concentration profiles inside the reactor they observed that the laminar flow becomes unstable at a Reynolds number around 900, and mixing was efficient in the 180° sharp turns inside the reactor due to the formation of vortices.

Imoberdorf et al. [171] determined the LVREA inside a fluidized bed photoreactor using a Monte Carlo approach to track the photons. They have considered the shadowing effect of the spheres, absorption of radiation by the TiO_2-coated particles and reflection by the spheres. It was found that operating the bed at low expansions resulted in the effective absorption of the radiation. Chen et al. [173] evaluated the internal and external mass transfer resistances for the immobilized TiO_2 photoreactor, used for the degradation of benzoic acid. Their results indicate that, although the external mass transfer resistance can be minimized by increasing the velocity of the flow field (i.e., the Reynolds number), the internal mass transfer was limited by the TiO_2 film thickness. They observed the optimum catalyst layer thickness to be 5 μm, above which there was no effect of mass transfer on the rate of reaction. This correlates to the discussion in the previous section, where the number of coating cycles was found to be detrimental to the degradation of the pollutants in immobilized catalyst systems. Dijkstra et al. [174] evaluated the effects of different parameters like radial dispersion, external mass transfer, flow rate, catalyst loading and oxygen concentration on the degradation of formic acid in different immobilized reactor configurations. Their results suggest that membrane and packed bed reactors show better performance compared to fiber and tubular reactors. Imoberdorf et al. [175] employed the kinetic information obtained from an 81 cm^2 flat plate lab scale photoreactor to model a 5209 cm^2 multi-annular, series flow, pilot-scale photoreactor, for the degradation of perchloroethylene. The model, based on the mass balance and radiation transport equations, without any adjustable parameters, was able to predict the experimental conversion of perchloroethylene within an error limit of 5.6%. Thus, modeling of photocatalytic reactors is important for performance assessment, optimal design and scaling up, in large-scale industrial applications.

11 Concluding Remarks

In this comprehensive review, we have covered the fundamental aspects of photocatalysis as applied to the degradation of water pollutants. Over the past two decades, nano-sized TiO_2 has emerged as a leading photocatalyst with the potential to catalyze the degradation and mineralization of a wide range of toxic organic compounds, such as chlorinated organics, phenolics, dyes, pesticides and herbicides, surfactants, pharmaceutical compounds and drugs and microorganisms. The current trend in photocatalysis research is aimed at extending the spectral absorption of pristine or bare TiO_2 to the visible region, better harvesting solar radiation. Toward realizing this goal, many modified forms of TiO_2, such as anion-

substituted TiO_2, dye-sensitized TiO_2 and heterostructured-TiO_2, have produced encouraging results.

One of the difficulties faced by the photocatalysis community is that TiO_2 synthesized by different protocols exhibit different physicochemical properties and substrate specific photoactivities and, hence, a single photocatalytic test with a specific material is not representative of its behavior for a wide class of organic compounds. Ryu and Choi [32] conducted the photocatalytic degradation of 19 test substances belonging to different classes of organic compounds using eight commercial TiO_2 samples, and concluded that each TiO_2 sample exhibits better photocatalytic activity compared to others for each class of organic compounds. Only DP-25 TiO_2 exhibited a better photoactivity for most of the organic compounds and can therefore be regarded as a yardstick for the assessment of the activity of novel photocatalytic materials. Therefore, owing to the ever increasing number of publications in this research area, the goal is to standardize the procedures, test substrates and photocatalytic activity, in order to have a rational comparison of the results of the different studies. Moreover, testing the degradation behavior of a single substrate is not representative of the "real" waste water or an effluent from a chemical plant. Hence, a degradation study of the multicomponent systems is a prospective research area. Although it is well-documented that the presence of humic substances, organic solvents, and chloride, sulfate and phosphate species retard the rate of degradation of organic compounds, evaluation of the degradation of systems with two or more organic compounds, metal ions or microorganisms is a relatively less explored topic.

The industrial viability of photocatalysis is driving research in the development of immobilized catalysts and photocatalytic reactors. In this venture, kinetic modeling of the reaction and reactor assumes paramount importance in the evaluation of the various rate limiting factors, optimum reaction conditions and scaling of reactors for the degradation of organic compounds. Currently, the large-scale applicability of photocatalysis for the degradation of organic pollutants is hindered by the costs involved in the operation of the treatment plant. Hence, more research in the selection of materials for the design of equipments and cheaper ways of catalyst synthesis and immobilization procedures is the key for further development. The authors do believe that exciting research opportunities exist in this field in the years to come.

References

1. Fujishima A, Honda K (1972) Electrochemical photolysis of water at a semiconductor electrode. Nature 238:37–38
2. Frank SN, Bard AJ (1977) Heterogeneous photocatalytic oxidation of cyanide and sulfite in aqueous solutions at semiconductor powders. J Phys Chem 81:1484–1488
3. Hsiao C-Y, Lee C-L, Ollis DF (1983) Heterogeneous photocatalysis: degradation of dilute solutions of dichloromethane (CH_2Cl_2), chloroform ($CHCl_3$) and carbon tetrachloride (CCl_4) with illuminated TiO_2 photocatalyst. J Catal 82:418–423

4. Pruden AL, Ollis DF (1983) Heterogeneous photocatalysis: the degradation of trichloroethylene in water. J Catal 82:404–417
5. Matsunaga T, Tomato R, Nakajima T, Wake H (1985) Photoelectrochemical sterilization of microbial cells by semiconductor powders. FEMS Microbiol Lett 29:211–214
6. O'Regan B, Grätzel M (1991) A low-cost, high efficiency solar cell based on dye-sensitized colloidal TiO_2 films. Nature 353:737–740
7. Fox MA, Dulay MT (1993) Heterogeneous photocatalysis. Chem Rev 93:341–357
8. Hoffmann MR, Martin ST, Choi W, Bahnemann DW (1995) Environmental applications of semiconductor photocatalysis. Chem Rev 95:69–96
9. Linsebigler AL, Lu G, Yates JT (1995) Photocatalysis on TiO_2 surfaces: principles, mechanisms and selected results. Chem Rev 95:735–758
10. Mills A, Hunte SL (1997) An overview of semiconductor photocatalysis. J Photochem Photobiol A: Chem 108:1–35
11. Fujishima A, Rao TN, Tryk DA (2000) Titanium dioxide photocatalysis. J Photochem Photobiol C: Photochem Rev 1:1–21
12. Carp O, Huisman CL, Reller A (2004) Photoinduced reactivity of titanium dioxide. Prog Solid State Chem 32:33–177
13. Fujishima A, Zhang X, Tryk DA (2008) TiO_2 photocatalysis and surface related phenomena. Surf Sci Rep 63:515–582
14. Chen X, Mao SS (2007) Titanium dioxide nanomaterials: synthesis, applications, modifications and applications. Chem Rev 107:2891–2959
15. Legrini O, Oliveros E, Braun AM (1993) Photochemical processes for water treatment. Chem Rev 93:671–698
16. Herrmann J-M (1999) Heterogeneous photocatalysis: fundamentals and applications to the removal of various types of aqueous pollutants. Catal Today 53:115–129
17. Bhatkhande DS, Pangarkar VG, Beenackers (2001) AACM Photocatalytic degradation for environmental applications—a review. J Chem Technol Biotechnol 77:102–116
18. Kabra K, Chaudhary R, Sawhney RL (2004) Treatment of hazardous organic and inorganic compounds through aqueous-phase photocatalysis: a review. Ind Eng Chem Res 43: 7683–7696
19. Zhao J, Chen C, Ma W (2005) Photocatalytic degradation of organic pollutants under visible light irradiation. Top Catal 35:269–278
20. Gaya UI, Abdullah AH (2008) Heterogeneous photocatalytic degradation of organic contaminants over titanium dioxide: a review of fundamentals, progress and problems. J Photochem Photobiol C: Photochem Rev 9:1–12
21. Malato S, Fernández-Ibáñez P, Maldonado MI, Blanco J, Gernjak W (2009) Decontamination and disinfection of water by solar photocatalysis: recent overview and trends. Catal Today 147:1–59
22. Wada Y, Yin H, Yanagida S (2002) Environmental remediation using catalysis driven under electromagnetic irradiation. Catal Sur Japan 5:127–138
23. Zhang Q, Gao L (2006) One-step preparation of size-defined aggregates of TiO_2 nanocrystals with tuning of their phase and composition. J Eur Ceram Soc 26:1535–1545
24. Sato S, Oimatsu S, Takahashi R, Sodesawa T, Nozaki F (1997) Pore size regulation of TiO_2 by use of a complex of titanium tetraisopropoxide and stearic acid. Chem Commun 22:2219-2220
25. Addamo M, Augugliaro V, Paola AD, García-López E, Loddo V, Marcí G, Molinari R, Palmisano L, Schiavello M (2004) Preparation, characterization and photoactivity of polycrystalline nanostructured TiO_2 catalysts. J Phys Chem B 108:3303–3310
26. Nagaveni K, Hegde MS, Ravishankar N, Subbanna GN, Madras G (2004) Synthesis and structure of nanocrystalline TiO_2 with lower band gap showing high photocatalytic activity. Langmuir 20:2900–2907
27. Mohamed MM, Bayoumy WA, Khairy M, Mousa MA (2007) Synthesis of micro-mesoporous TiO_2 materials assembled via cationic surfactants: morphology, thermal stability and surface acidity characteristics. Micropor Mesopor Mater 103:174–183

28. Venkatachalam N, Palanichamy M, Murugesan V (2007) Sol-gel preparation and characterization of nanosize TiO_2: its photocatalytic performance. Mater Chem Phys 104:454–459
29. Dong X, Tao J, Li Y, Zhu H (2010) Oriented single crystalline TiO_2 nano-pillars directly grown on titanium substrate in tetramethylammonium hydroxide solution. Appl Surf Sci 256:2532–2538
30. Cheng Y, Sun H, Jin W, Xu N (2007) Photocatalytic degradation of 4-chlorophenol with combustion synthesized TiO_2 under visible light irradiation. Chem Eng J 128:127–133
31. Zhang Z, Wang C-C, Zakaria R, Ying JY (1998) Role of particle size in nanocrystalline TiO_2-based photocatalysts. J Phys Chem B 102:10871–10878
32. Ryu J, Choi W (2008) Substrate-specific photocatalytic activities of TiO_2 and multiactivity test for water treatment application. Environ Sci Technol 42:294–300
33. Hidalgo MC, Colón G, Navío JA (2002) Modification of the physicochemical properties of commercial TiO_2 samples by soft mechanical activation. J Photochem Photobiol A: Chem 148:341–348
34. Hathway T, Jenks WS (2008) Effects of sintering of TiO_2 particles on the mechanisms of photocatalytic degradation of organic molecules in water. J Photochem Photobiol A: Chem 200:216–224
35. Kritikos DE, Xekoukoulotakis NP, Psillakis E, Mantzavinos D (2007) Photocatalytic degradation of reactive black 5 in aqueous solutions: effect of operating conditions and coupling with ultrasound irradiation. Water Res 41:2236–2246
36. Sivalingam G, Nagaveni K, Hegde MS, Madras G (2003) Photocatalytic degradation of various dyes by combustion synthesized nano anatase TiO_2. Appl Catal B: Environ 45:23–38
37. Aarthi T, Madras G (2007) Photocatalytic degradation of rhodamine dyes with nano-TiO_2. Ind Eng Chem Res 46:7–14
38. Vinu R, Akki SU, Madras G (2010) Investigation of dye functional group on the photocatalytic degradation of dyes by nano-TiO_2. J Hazard Mater 176:765–773
39. Sivalingam G, Priya MH, Madras G (2004) Kinetics of photodegradation of substituted phenols by solution combustion synthesized TiO_2. Appl Catal B: Environ 51:67–76
40. Priya MH, Madras G (2006) Kinetics of photocatalytic degradation of phenols with multiple substituent groups. J Photochem Photobiol A: Chem 179:256–262
41. Priya MH, Madras G (2006) Photocatalytic degradation of nitrobenzenes with combustion synthesized nano-TiO_2. J Photochem Photobiol A: Chem 178:1–7
42. Vijayalakshmi SP, Madras G (2006) Photocatalytic degradation of poly(ethylene oxide) and polyacrylamide. J Appl Polym Sci 100:3997–4003
43. Sivalingam G, Madras G (2004) Photocatalytic degradation of poly(bisphenol-A-carbonate) in solution over combustion-synthesized TiO_2: mechanism and kinetics. Appl Catal A: Gen 269:81–90
44. Aarthi P, Madras G (2008) Photocatalytic reduction of metals in presence of combustion synthesized nano-TiO_2. Catal Commun 9:630–634
45. Ollis DF, Pelizzetti E, Serpone N (1991) Photocatalyzed destruction of water contaminants. Environ Sci Technol 25:1522–1529
46. Blake DM (2001) Bibliography of work on the heterogeneous photocatalytic removal of hazardous compounds from water and air. NREL/TP-510-31319, National Renewable Energy Laboratory, Golden
47. Li X, Cubbage JW, Jenks WS (1999) Photocatalytic degradation of 4-chlorophenol. 2. The 4-chlorocatechol pathway. J Org Chem 64:8525–8536
48. Rajeshwar K, Osugi ME, Chanmanee W, Chenthamarakshan CR, Zanoni MVB, Kajitvichyanukul P, Krishnan-Ayer R (2008) Heterogeneous photocatalytic treatment of organic dyes in air and aqueous media. J Photochem Photobiol C: Photochem Rev 9:171–192
49. Rauf MA, Ashraf SS (2009) Fundamental principles and application of heterogeneous photocatalytic degradation of dyes in solution. Chem Eng J 151:10–18

50. Konstantinou IK, Albanis TA (2004) TiO_2-assisted photocatalytic degradation of azo dyes in aqueous solution: kinetic and mechanistic investigations: a review. Appl Catal B: Environ 49:1–14
51. Akpan UG, Hameed BH (2009) Parameters affecting the photocatalytic degradation of dyes using TiO_2-based photocatalysts: a review. J Hazard Mater 170:520–529
52. Han F, Kambala VSR, Srinivasan M, Rajarathnam D, Naidu R (2009) Tailored titanium dioxide photocatalysts for the degradation of organic dyes in wastewater treatment: a review. Appl Catal A: Gen 359:25–40
53. Houas A, Lachheb H, Ksibi M, Elaloui E, Guillard C, Herrmann J-M (2001) Photocatalytic degradation pathway of methylene blue in water. Appl Catal B: Environ 31:145–157
54. Epling GA, Lin C (2002) Photoassisted bleaching of dyes utilizing TiO_2 and visible light. Chemosphere 46:561–570
55. Silva CG, Wang W, Faria JL (2006) Photocatalytic and photochemical degradation of mono-, di- and tri-azo dyes in aqueous solution under UV irradiation. J Photochem Photobiol A: Chem 181:314–324
56. Stylidi M, Kondarides DI, Verykios XE (2003) Pathways of solar light-induced photocatalytic degradation of azo dyes in aqueous TiO_2 suspensions. Appl Catal B: Environ 40:271–286
57. Sleiman M, Vildozo D, Ferronato C, Chovelon J-M (2007) Photocatalytic degradation of azo dye Metanil Yellow: optimization and kinetic modeling using a chemometric approach. Appl Catal B: Environ 77:1–11
58. Hu C, Yu JC, Hao Z, Wong PK (2003) Photocatalytic degradation of triazine-containing azo dyes in aqueous TiO_2 suspensions. Appl Catal B: Environ 42:47–55
59. Saquib M, Muneer M (2002) Semiconductor mediated photocatalyzed degradation of an anthraquinone dye, Remazol Brilliant Blue R under sunlight and artificial light source. Dyes Pigments 53:237–249
60. Vautier M, Guillard C, Herrmann J-M (2001) Photocatalytic degradation of dyes in water: case study of indigo and of indigo carmine. J Catal 201:46–59
61. Wu T, Liu G, Zhao J, Hidaka H, Serpone N (1998) Photoassisted degradation of dye pollutants. V. Self-photosensitized oxidative transformation of Rhodamine B under visible light irradiation in aqueous TiO_2 dispersions. J Phys Chem B 102:5845–5851
62. Park H, Choi W (2005) Photocatalytic reactivities of nafion-coated TiO_2 for the degradation of charged organic compounds under UV or visible light. J Phys Chem B 109:11667–11674
63. Chen C-C, Lu C-S (2007) Mechanistic studies of the photocatalytic degradation of Methyl Green: an investigation of products of the decomposition processes. Environ Sci Technol 41:4389–4396
64. Konstantinou IK, Zarkadis AK, Albanis TA (2001) Photodegradation of selected herbicides in various natural waters and soils under environmental conditions. J Environ Qual 30:121–130
65. Zhu X, Yuan C, Bao Y, Yang J, Wu Y (2005) Photocatalytic degradation of pesticide pyridaben on TiO_2 particles. J Mol Catal A: Chem 229:95–105
66. Wei L, Shifu C, Wei Z, Sujuan Z (2009) Titanium dioxide mediated photocatalytic degradation of methamidophos in aqueous phase. J Hazard Mater 164:154–160
67. Moctezuma E, Leyva E, Palestino G, de Lasa H (2007) Photocatalytic degradation of methyl parathion: reaction pathways and intermediate reaction products. J Photochem Photobiol A: Chem 186:71–84
68. Lhomme L, Brosillon S, Wolbert D (2007) Photocatalytic degradation of a triazole pesticide, cyproconazole, in water. J Photochem Photobiol A: Chem 188:34–42
69. Yu B, Zeng J, Gong L, Zhang M, Zhang L, Chen X (2007) Investigation of the photocatalytic degradation of organochlorine pesticides on a nano-TiO_2 coated film. Talanta 72:1667–1674
70. Navarro S, Fenoll J, Vela N, Ruiz E, Navarro G (2009) Photocatalytic degradation of eight pesticides in leaching water by use of ZnO under natural sunlight. J Hazard Mater 172:1303–1310

71. Aungpradit T, Sutthivaiyakit P, Martens D, Sutthivaiyakit S, Kettrup AAF (2007) Photocatalytic degradation of triazophos in aqueous titanium dioxide suspension: identification of intermediates and degradation pathways. J Hazard Mater 146:204–213
72. Molinari R, Pirillo F, Loddo V, Palmisano L (2006) Heterogeneous photocatalytic degradation of pharmaceuticals in water by using polycrystalline TiO_2 and a nanofiltration membrane reactor. Catal Today 118:205–213
73. Chatzitakis A, Berberidou C, Paspaltsis I, Kyriakou G, Sklaviadis T, Poulios I (2008) Photocatalytic degradation and drug activity reduction of chloramphenicol. Water Res 42:386–394
74. Abellán MN, Bayarri B, Giménez J, Costa J (2007) Photocatalytic degradation of sulfamethoxazole in aqueous suspension of TiO_2. Appl Catal B: Environ 74:233–241
75. An T, Yang H, Li G, Song W, Cooper WJ, Nie X (2010) Kinetics and mechanism of advanced oxidation processes (AOPs) in degradation of ciprofloxacin in water. Appl Catal B: Environ 94:288–294
76. Radjenović J, Sirtori C, Petrović M, Barceló D, Malato S (2009) Solar photocatalytic degradation of persistent pharmaceuticals at pilot-scale: kinetics and characterization of major intermediate products. Appl Catal B: Environ 89:255–264
77. Méndez-Arriaga F, Esplugas S, Giménez J (2008) Photocatalytic degradation of non-steroidal anti-inflammatory drugs with TiO_2 and simulated solar irradiation. Water Res 42:585–594
78. Calza P, Sakkas VA, Medana C, Baiocchi C, Dimou A, Pelizzetti E, Albanis T (2006) Photocatalytic degradation study of diclofenac over aqueous TiO_2 suspensions. Appl Catal B: Environ 67:197–205
79. Sakkas VA, Calza P, Medana C, Villioti AE, Baiocchi C, Pelizzetti E, Albanis T (2007) Heterogeneous photocatalytic degradation of the pharmaceutical agent salbutamol in aqueous titanium dioxide suspensions. Appl Catal B: Environ 77:135–144
80. Calza P, Massolino C, Monaco G, Medana C, Baiocchi C (2008) Study of the photolytic and photocatalytic transformation of amiloride in water. J Pharm Biomed Anal 48:315–320
81. Cheng YW, Chan RCY, Wong (2007) Disinfection of *Legionella pneumophila* by photocatalytic oxidation. Water Res 41:842–852
82. Ibáñez JA, Litter AI, Pizarro RA (2003) Photocatalytic bactericidal effect of TiO_2 on *Enterobacter cloacae*: comparative study with other gram (−) bacteria. J Photochem Photobiol A:Chem 157:81–85
83. Prasad GK, Agarwal GS, Singh B, Rai GP, Vijayaraghavan R (2009) Photocatalytic inactivation of *Bacillus anthracis* by titania nanomaterials. J Hazard Mater 165:506–510
84. Liu H-L, Yang TC-K (2003) Photocatalytic inactivation of *Escherichia coli* and *Lactobacillus helveticus* by ZnO and TiO_2 activated with ultraviolet light. Process Biochem 39:475–481
85. Kubacka A, Ferrer M, Martínez-Arias A, Fernández-García M (2008) Ag promotion of TiO_2-anatase disinfection capability: study of *Escherichia coli* inactivation. Appl Catal B: Environ 84:87–93
86. Hu C, Guo J, Qu J, Hu X (2007) Photocatalytic degradation of pathogenic bacteria with AgI/TiO_2 under visible light irradiation. Langmuir 23:4982–4987
87. Wu T-S, Wang K-X, Li G-D, Sun S-Y, Sun J, Chen J-S (2010) Montmorillonite-supported Ag/TiO_2 nanoparticles: an efficient visible-light bacteria photodegradation material. ACS Appl Mater Interf 2:544–550
88. Wu P, Xie R, Imlay JA, Shang JK (2009) Visible-light-induced photocatalytic inactivation of bacteria by composite photocatalysts of palladium oxide and nitrogen-doped titanium oxide. Appl Catal B: Environ 88:576–581
89. Yu JC, Ho W, Yu J, Yip H, Wong PK, Zhao J (2005) Efficient visible-light-induced photocatalytic disinfection on sulfur-doped nanocrystalline titania. Environ Sci Technol 39:1175–1179

90. Pelaez M, de la Cruz AA, Stathatos E, Falaras P, Dionysiou DD (2009) Visible light-activated N–F-codoped TiO_2 nanoparticles for the photocatalytic degradation of microcystin-LR in water. Catal Today 144:19–25
91. Cho M, Chung H, Choi W, Yoon J (2004) Linear correlation between inactivation of *E. coli* and OH radical concentration in TiO_2 photocatalytic disinfection. Water Res 34:1069–1077
92. Matsunaga T, Tomoda R, Nakajima T, Nakamura N, Komine T (1988) Continuous-sterilization system that uses photosemiconductor powders. Appl Environ Microbiol 54:1330–1333
93. Saito T, Iwase T, Horie J, Morioka T (1992) Mode of photocatalytic bactericidal action of powdered semiconductor TiO_2 on mutans streptococci. J Photochem Photobiol B: Biol 14:369–379
94. Maness P-C, Smolinski S, Blake DM, Hyang Z, Wolfrum EJ, Jacoby WA (1999) Bactericidal activity of photocatalytic TiO_2 reaction: toward an understanding of its killing mechanism. Appl Environ Microbiol 65:4094–4098
95. Rincón A-G, Pulgarin C (2004) Effect of pH, inorganic ions, organic matter and H_2O_2 on *E. coli* K12 photocatalytic inactivation by TiO_2: implications in solar water ds infection. Appl Catal B: Environ 51:283–302
96. Pal A, Pehkonen SO, Yu LE, Ray MB (2008) Photocatalytic inactivation of airborne bacteria in a continuous-flow reactor. Ind Eng Chem Res 47:7580–7585
97. Sharma VK, Yngard RA, Lin Y (2009) Silver nanoparticles: green synthesis and their antimicrobial activities. Adv Coll Interf Sci 145:83–96
98. Naeem K, Weiqian P, Ouyang F (2010) Thermodynamic parameters of activation for photodegradation of phenolics. Chem Eng J 156:505–509
99. Madras G, Smith JM, McCoy BJ (1996) Thermal degradation of poly(α-methyl styrene) in solution. Polym Degrad Stab 52:349–358
100. Devi LG, Murthy BN, Kumar SG (2009) Heterogeneous photo catalytic degradation of anionic and cationic dyes over TiO_2 and TiO_2 doped with Mo^{6+} ions under solar light: correlation of dye structure and its adsorptive tendency on the degradation rate. Chemosphere 76:1163–1166
101. Alrousan DMA, Dunlop PSM, McMurray TA, Byrne JA (2009) Photocatalytic inactivation of *E. coli* in surface water using immobilized nanoparticle TiO_2 films. Water Res 43:47–54
102. Matthews RW, McEvoy SR (1992) A comparison of 254 and 350 nm excitation of TiO_2 in simple photocatalytic reactors. J Photochem Photobiol A: Chem 66:355–366
103. Kuhn HJ, Braslavsky SE, Schmidt R (2004) Chemical actinometry. Pure Appl Chem 76:2105–2146
104. Meng Y, Huang X, Wu Y, Wang X, Qian Y (2002) Kinetic study and modeling on photocatalytic degradation of para-chlorobenzoate at different light intensities. Environ Poll 117:307–313
105. Wu C-H, Chern J-M (2006) Kinetics of photocatalytic decomposition of methylene blue. Ind Eng Chem Res 45:6450–6457
106. Lim LLP, Lynch RJ, In S-I (2009) Comparison of simple and economical photocatalyst immobilization procedures. Appl Catal A: Gen 365:214–221
107. Epling GA, Lin C (2002) Investigation of retardation effects on the titanium dioxide photodegradation system. Chemosphere 46:937–944
108. Azevedo EB, Neto FRA, Dezotti M (2004) TiO_2-photocatalyzed degradation of phenol in saline media: lumped kinetics, intermediates and acute toxicity. Appl Catal B: Environ 54:165–173
109. Chen D, Ray AK (2001) Removal of toxic metal ions from wastewater by semiconductor photocatalysis. Chem Eng Sci 56:1561–1570
110. Prairie MR, Evans LR, Stange BM, Martinez SL (1993) An investigation of TiO_2 photocatalysis for the treatment of water contaminated with metals and organic chemicals. Environ Sci Technol 27:1776–1782

111. Chen C, Li X, Ma W, Zhao J, Hidaka H, Serpone N (2002) Effect of transition metal ions on the TiO_2-assisted photodegradation of dyes under visible irradiation: a probe for interfacial electron transfer process and reaction mechanism. J Phys Chem B 106:318–324
112. Kyung H, Lee J, Choi W (2005) Simultaneous and synergistic conversion of dyes and heavy metal ions in aqueous TiO_2 suspensions under visible-light illumination. Environ Sci Technol 39:2376–2382
113. Wang N, Chen Z, Zhu L, Jiang X, Lv B, Tang H (2007) Synergistic effects of cupric and fluoride ions on photocatalytic degradation of phenol. J Photochem Photobiol A: Chem 191:193–200
114. Vinu R, Madras G (2008) Kinetics of simultaneous photocatalytic degradation of phenolic compounds and reduction of metal ions with nano-TiO_2. Environ Sci Technol 42:913–919
115. Sun B, Reddy EP, Smirniotis PG (2005) Visible light Cr(VI) reduction and organic chemical oxidation by TiO_2 photocatalysis. Environ Sci Technol 39:6251–6259
116. Turchi CS, Ollis DF (1990) Photocatalytic degradation of organic water contaminants: mechanisms involving hydroxyl radical attack. J Catal 122:178–192
117. Li Y, Sun S, Ma M, Ouyang Y, Yan W (2008) Kinetic study and model of the photocatalytic degradation of rhodamine B(RhB) by a TiO_2-coated activated carbon catalyst: effects of initial RhB content, light intensity and TiO_2 content in the catalyst. Chem Eng J 142:147–155
118. Almquist CB, Biswas P (2001) A mechanistic approach to modeling the effect of dissolved oxygen in photo-oxidation reactions on titanium dioxide in aqueous systems. Chem Eng Sci 56:3421–3430
119. Benabbou AK, Derriche Z, Felix C, Lejeune P, Guillard C (2007) Photocatalytic inactivation of *Escherischia coli*: effect of concentration of TiO_2 and microorganism, nature and intensity of UV irradiation. Appl Catal B: Environ 76:257–263
120. Marugán J, van Grieken R, Sordo C, Cruz C (2008) Kinetics of photocatalytic disinfection of *Escherichia coli* suspensions. Appl Catal B: Environ 82:27–36
121. Labas MD, Brandi RJ, Martín CA, Cassano AE (2006) Kinetics of bacteria inactivation employing UV radiation under clear water conditions. Chem Eng J 121:135–145
122. Marugán J, van Griekan R, Pablos C, Sordo C (2010) Anologies and differences between photocatalytic oxidation of chemicals and photocatalytic inactivation of microorganisms. Water Res 44:789–796
123. Priya MH, Madras G (2006) Kinetics of photocatalytic degradation of chlorophenol, nitrophenol and their mixtures. Ind Eng Chem Res 45:482–486
124. Aarthi P, Narahari P, Madras G (2007) Photocatalytic degradation of azure and sudan dyes using nano-TiO_2. J Hazard Mater 149:725–734
125. Levenspiel O (1999) Chemical reaction engineering. John Wiley, Singapore
126. Choi W, Termin A, Hoffmann MR (1994) The role of metal ion dopants in quantum-sized TiO_2: correlation between photoreactivity and charge carrier recombination dynamics. J Phys Chem 98:13669–13679
127. Serpone N, Lawless D, Disdier J, Herrmann J-M (1994) Spectroscopic, photoconductivity, and photocatalytic studies of TiO_2 colloids: naked and with the lattice doped with Cr^{3+}, Fe^{3+} and V^{5+} cations. Langmuir 10:643–652
128. Shah SI, Li W, Huang C-P, Jung O, Ni C (2002) Study of Nd^{3+}, Pd^{2+}, Pt^{4+} and Fe^{3+} dopant effect on photoreactivity of TiO_2 nanoparticles. Proc Nat Acad Sci 99:6482–6486
129. Dvoranová D, Brezová V, Mazúr M, Malati MA (2002) Investigations of metal-doped titanium dioxide photocatalysts. Appl Catal B: Environ 37:91–105
130. Nagaveni K, Hegde MS, Madras G (2004) Structure and photocatalytic activity of $Ti_{1-x}M_xO_{2\pm\delta}$ (M = W, V, Ce, Zr, Fe, and Cu) synthesized by solution combustion method. J Phys Chem B 108:20204–20212
131. Štengl V, Bakardjieva S, Murafa N (2009) Preparation and photocatalytic activity of rare earth doped TiO_2 nanoparticles. Mater Chem Phys 114:217–226

132. Roy S, Hegde MS, Ravishankar N, Madras G (2007) Creation of redox adsorption sites by Pd^{2+} ion substitution in nano TiO_2 for high photocatalytic activity of CO oxidation, NO reduction and NO decomposition. J Phys Chem C 111:8153–8160
133. Vinu R, Madras G (2008) Synthesis and photoactivity of Pd substituted nano-TiO_2. J Mol Catal A: Chem 291:5–11
134. Paola AD, García-López E, Ikeda S, Marcí G, Ohtani B, Palmisano L (2002) Photocatalytic degradation of organic compounds in aqueous systems by transition metal doped polycrystalline TiO_2. Catal Today 75:87–93
135. Vinu R, Madras G (2009) Photocatalytic activity of Ag-substituted and impregnated nano-TiO_2. Appl Catal A: Gen 366:130–140
136. Asahi R, Morikawa T, Ohwaki T, Aoki K, Taga Y (2002) Visible-light photocatalysis in nitrogen-doped titanium oxides. Science 293:269–271
137. Khan SUM, Al-Shahry M, Ingler WB Jr (2002) Efficient photochemical water splitting by a chemically modified *n*-TiO_2. Science 297:2243–2245
138. Liu G, Wang L, Yang HG, Cheng H-M, Lu GQM (2010) Titania-based photocatalysts–crystal growth, doping and heterostructuring. J Mater Chem 20:831–843
139. Serpone N (2006) Is the band gap of pristine TiO_2 narrowed by anion- and cation-doping of titanium dioxide in second-generation photocatalysts? J Phys Chem B 110:24287–24293
140. Nagaveni K, Sivalingam G, Hegde MS, Madras G (2004) Solar photocatalytic degradation of dyes: high activity of combustion synthesized nano TiO_2. Appl Catal B: Environ 48:83–93
141. Xiao Q, Zhang J, Xiao C, Si Z, Tan X (2008) Solar photocatalytic degradation of methylene blue in carbon-doped TiO_2 nanoparticles suspension. Sol Energy 82:706–713
142. Zhong J, Chen F, Zhang J (2010) Carbon-deposited TiO_2: synthesis, characterization and visible photocatalytic performance. J Phys Chem C 114:933–939
143. Ao Y, Xu J, Fu D, Yuan C (2009) Synthesis of C, N, S-tridoped mesoporous titania with enhanced visible light-induced photocatalytic activity. Micropor Mesopor Mater 122:1–6
144. Yu T, Tan X, Zhao L, Yin Y, Chen P, Wei J (2009) Characterization, activity and kinetics of a visible light driven photocatalyst: cerium and nitrogen co-doped TiO_2 particles. Chem Eng J. doi: 10.1016/j.cej.2009.10.051
145. Ho W, Yu JC, Lin J, Yu J, Li P (2004) Preparation and photocatalytic behavior of MoS_2 and WS_2 nanocluster sensitized TiO_2. Langmuir 20:5865–5869
146. Wang D, Zhang J, Luo Q, Li X, Duan Y, An J (2009) Characterization and photocatalytic activity of poly(3-hexyl thiophene)-modified TiO_2 for degradation of methyl orange under visible light. J Hazard Mater 169:546–550
147. Sun Q, Xu Y (2009) Sensitization of TiO_2 with aluminium phthalocyanine: factors influencing the efficiency for chlorophenol degradation in water under visible light. J Phys Chem C 113:12387–12394
148. Liang H-C, Li X-Z (2009) Visible-induced photocatalytic reactivity of polymer sensitized titania nanotube films. Appl Catal B: Environ 86:8–17
149. Xiangzhong L, Wei Z, Jincai Z (2002) Visible light-sensitized semiconductor photocatalytic degradation of 2, 4-dichlorophenol. Sci China Ser B 45:421–425
150. Gilma GO, Carlos APM, Fernando MO, Edgar AP-M (2005) Photocatalytic degradation of phenol on TiO_2 and TiO_2/Pt sensitized with matallophthalocyanines. Catal Today 107–108:589–594
151. Ross H, Bendig J, Hecht S (1994) Sensitized photocatalytical oxidation of terbutylazine. Solar Energy Mater Solar Cells 33:475–481
152. Granados-Oliveros G, Páez-Mozo EA, Ortega FM, Ferronato C, Chovelon J-M (2009) Degradation of atrazine using metalloporphyrins supported on TiO_2 under visible light irradiation. Appl Catal B: Environ 89:448–454
153. Bae E, Choi W (2003) Highly enhanced photoreductive degradation of perchlorinated compounds on dye-sensitized metal/TiO_2 under visible light. Environ Sci Technol 37:147–152

154. Li G-S, Zhang D-Q, Yu JC (2009) A new visible-light photocatalyst: CdS quantum dots embedded mesoporous TiO_2. Environ Sci Technol 43:7079–7085
155. Chiou C-S, Shie J-L, Chang C-Y, Liu C-C, Chang C-T (2006) Degradation of di-*n*-butyl phthalate using photoreactor packed with TiO_2 immobilized on glass beads. J Hazard Mater B 137:1123–1129
156. Horikoshi S, Watanabe N, Onishi H, Hidaka H, Serpone N (2002) Photodecomposition of a nonylphenol polyethoxylate surfactant in a cylindrical photoreactor with TiO_2 immobilized fiberglass cloth. Appl Catal B: Environ 37:117–129
157. Lee J-M, Kim M-S, Kim B-W (2004) Photodegradation of bisphenol-A with TiO_2immobilized on the glass tubes including the UV light lamps. Water Res 38:3605–3613
158. Tryba B (2008) Immobilization of TiO_2 and Fe-C-TiO_2 photocatalysts on the cotton material for application in a flow photocatalytic reactor for decomposition of phenol in water. J Hazard Mater 151:623–627
159. Chen Y, Dionysiou DD (2007) A comparative study on physicochemical properties and photocatalytic behavior of macroporous TiO_2–P25 composite films and macroporous TiO_2 films coated on stainless steel substrate. Appl Catal A: Gen 317:129–137
160. Zhang Q, Fan W, Gao L (2007) Anatase TiO_2 nanoparticles immobilized on ZnO tetrapods as a highly efficient and easily recyclable photocatalyst. Appl Catal B: Environ 76:168–173
161. Gao Y, Liu H (2005) Preparation and catalytic property study of a novel kind of suspended photocatalyst of TiO_2-activated carbon immobilized on silicone rubber film. Mater Chem Phys 92:604–608
162. Nakashima T, Ohko Y, Tryk DA, Fujishima A (2002) Decomposition of endocrine-disrupting chemicals in water by use of TiO_2 photocatalysts immobilized on polytetrafluoroethylene mesh sheets. J Photochem Photobiol A: Chem 151:207–212
163. Magalhães F, Lago RM (2009) Floating photocatalysts based on TiO_2 grafted on expanded polystyrene beads for the solar degradation of dyes. Sol Energy 83:1521–1526
164. Faramarzpour M, Vossoughi M, Borghei M (2009) Photocatalytic degradation of furfural by titania nanoparticles in a floating-bed photoreactor. Chem Eng J 146:79–85
165. Rachel A, Lavedrine B, Subrahmanyam M, Boule P (2002) Use of porous lavas as supports of photocatalysis. Catal Commun 3:165–171
166. Grieken RV, Marugán J, Sordo C, Pablos C (2009) Comparison of the photocatalytic disinfection of *E. coli* suspensions in slurry, wall and fixed-bed reactors. Catal Today 144:48–54
167. Rao KVS, Subrahmanyam M, Boule P (2004) Immobilized TiO_2 photocatalyst during long-tem use: decrease of activity. Appl Catal B: Environ 49:239–249
168. Lasa H, Serrano B, Salaices M (2005) Photocatalytic reaction engineering. Springer, New York
169. Puma GL, Yue PL (2001) A novel fountain photocatalytic reactor: model development and experimental validation. Chem Eng Sci 56:2733–2744
170. Denny F, Scott J, Pareek V, Peng GD, Amal R (2009) CFD modeling for a TiO_2-coated glass-bead photoreactor irradiated by optical fibres: photocatalytic degradation of oxalic acid. Chem Eng Sci 64:1695–1706
171. Imoberdorf GE, Taghipour F, Keshmiri M, Mohseni M (2008) Predictive radiative field modeling for fluidized bed photocatalytic reactors. Chem Eng Sci 63:4228–4238
172. Jarandehei A, Visscher AD (2009) Three-dimensional CFD model for a flat plate photocatalytic reactor: degradation of TCE in a serpentine flow field. AIChE J 55:312–320
173. Chen D, Li F, Ray AK (2000) Effect of mass transfer and catalyst layer thickness on photocatalytic reaction. AIChE J 46:1034–1045
174. Dijkstra MFJ, Hoerts ECB, Beenackers AACM, Wesselingh JA (2003) Performance of immobilized photocatalytic reactors in continuous mode. AIChE J 49:734–744
175. Imoberdorf GE, Irazoqui HA, Alfano OM, Cassano AE (2007) Scaling-up from first principles of a photocatalytic reactor for air pollution remediation. Chem Eng Sci 62: 793–804